Rheology study of ballast-sleeper interaction with particle image Velocimetry (PIV) and discrete element modelling (DEM)

Guo, Yunlong; Jia, Wenli; Markine, Valeri; Jing, Guoqing

DOI
10.1016/j.conbuildmat.2021.122710

Publication date
2021

Document Version
Accepted author manuscript

Published in
Construction and Building Materials

Citation (APA)
Guo, Y., Jia, W., Markine, V., & Jing, G. (2021). Rheology study of ballast-sleeper interaction with particle image Velocimetry (PIV) and discrete element modelling (DEM). *Construction and Building Materials*, *282*, 1-21. Article 122710. https://doi.org/10.1016/j.conbuildmat.2021.122710

Rheology study of ballast-sleeper interaction with Particle Image Velocimetry (PIV) and discrete element modelling (DEM)

Yunlong Guo [1], Wenli Jia [1], Valeri Markine [1], Guoqing Jing [2*]

1. Faculty of Civil Engineering and Geosciences, Delft University of Technology, Delft, 2628CN, Netherlands
2. School of Civil Engineering, Beijing Jiaotong University, Beijing, 100044, China
*. Corresponding author
Email addresses: gqjing@bjtu.edu.cn (G. Jing)

Abstract: Ballast rheology is a phenomenon that describes movements of ballast particles as the discrete nature, which eventually leads to the ballast bed fluid deformation after a long-time service. In most cases, ballast rheology is the main reason of track irregularity that leads to some track defects, e.g., hanging sleeper and mud spots. Therefore, it is significant to confirm the ballast rheology mechanism, which not only benefits for alleviating track defects, prolonging track service and providing safe transportation, but also provides an innovated means for accurately calibrating the discrete element method (DEM) models.

Towards this aim, the Particle Image Velocimetry (PIV) is utilised to study ballast rheology through measuring ballast particle displacements in the single sleeper push test (SSPT). The ballast rheology results are compared with those from the DEM SSPT model, through which the DEM model is calibrated. Results show that the PIV is an effective technical means for ballast rheology study and DEM model calibration. This study is helpful for the researchers to build more precise DEM models, further providing theoretical methodology for ballast track construction and innovation.

Key words: Ballast rheology; Ballasted track; PIV; Discrete element method; Calibration; Single sleeper push test

1. Introduction

The definition of ballast rheology consists of two aspects. On one hand, it means individual ballast particle movements (translation and rotation) that usually occur under train cyclic loadings [1]. On the other hand, the particle movements induce the slow flow of ballast assemblies (like liquid) from the overall view, especially at some special structures with high ballast vibrations, e.g. the ballast bed on bridges [2].

Due to the discrete nature of ballast assemblies, the inevitable particle movements cause ballast migration, further resulting in the plastic deformation of ballast bed (at lateral, longitudinal and vertical directions) [3-8]. Note that inhomogeneous plastic deformation is the main reason of hanging sleepers and mud spots [9-11], causing the irregular track geometry, frequent maintenances and safety problems [12, 13]. Consequently, confirming the ballast rheology mechanism and its effect factors are important for not only preventing inhomogeneous plastic deformation, but also alleviating track irregularities [14].

Nevertheless, limited experimental studies were performed in earlier literatures. In addition, the studies have not comprehensively revealed the mechanism. For instance, the SmartRock was utilised to measure the accelerations at three orthogonal directions and angular acceleration [9]. The SmartRock is a three-dimensional printed ballast particle with a triaxial accelerometer embedded inside. Using the SmartRock, individual ballast particle movements can be reflected from the

accelerations. It is able to measure particle accelerations at limited locations, but the particle displacements cannot be obtained. For this, it seems insufficient for the ballast rheology study.

Another study presented the ballast assembly rheology at the longitudinal direction in a full-size six-sleeper track model [1]. The PIV was utilised to measure the displacements of ballast particles under cyclic longitudinal loadings. The PIV is a technical means belonging to the digital image correlation. It analyses and measures the displacements of the same pixel between two images [2]. This study shows the feasibility of the PIV application to the ballast rheology study.

In [15], the PIV was used to confirm how many ballast particles moved when laterally pushing the sleeper. Yet, the study only provided the movements of ballast particles at the surface, which can be photographed. Improvements on using the PIV are needed to present the ballast rheology under ballast bed surface. For example, one cross section of ballast bed can be photographed and analysed with the PIV.

Regarding the numerical study on the ballast rheology, plenty of studies with the DEM were presented in the literatures [16-19]. Because using the DEM has several advantages, including 1) complete particle information acquisition (acceleration, velocity, displacement, contact force) [19-21], 2) modelling ballast particle properties (density, size, shape) [21-23] and 3) ballast degradation involvement (breakage and abrasion) [24, 25].

However, calibrating the particle movements in DEM model are still challenging until now [26]. Specifically, the particle movements are larger than real conditions due to the particle kinetic energy cannot be appropriately dissipated during the numerical calculation, causing unrealistic ballast rheology. In practise, energies (from loadings) applied to ballast assemblies are dissipated by the relative motions between ballast particles and particle degradation, i.e. sliding, rolling, breaking and wearing. Yet, most of DEM models are simplified for reducing calculation cost, and the contact model or the boundary condition are not properly adjusted. For these reasons, the particle movements are usually with large errors, causing the ballast assembly rheology cannot be well presented [27].

For example, most of the earlier DEM models, simple sphere or discs were utilised and the contact model between them is the linear contact model (contact model description in [27]) [28-30]. Moreover, the studies did not consider ballast degradation. The models with simple spheres (discs) have less contact numbers than real, and the parameters for the linear contact model have not been consentaneously developed [31]. Different models usually applied considerably different parameter values. Because the kinetic energies are dissipated at the contacts by sliding, less contact numbers result in accumulated energy. Because of energy accumulation, the ballast rheology cannot be realistically presented in DEM models.

Although in later studies, other contact models and non-sphere particles were utilised, the model was still calibrated and validated by matching the numerical results with some laboratory tests' results, e.g., direct shear test (force-displacement curve) and triaxial test (stress-strain curve) [3, 32-35]. In other words, since the two curves (from experimental or numerical) are closely matched, the model is validated.

Nevertheless, the DEM simulations are still needed for the ballast assembly rheology study, because it can measure and record all the particle movements (displacements). This is not easy to be obtained from the experimental tests (inside the ballast assemblies). More importantly, when the DEM models are well calibrated, they can provide detailed mesoscopic particle information (displacements, contact forces and accelerations) [16, 33, 36].

Towards this problem, combining the experimental test with DEM simulations were applied for ballast rheology study. For the experimental test, the single sleeper push test (SSPT) was performed, which is a widely-used approach to measure lateral resistance of ballast bed [37-39]. It needs to note that one side of the ballast bed is held by a glass wall for taking ballast bed images of cross section. The PIV was applied to measure and record the ballast displacements. With the test configurations and results, a DEM model of the SSPT was built. After comparing the experimental and numerical results of the particle displacements, the DEM SSPT model is validated. This study assists in establishing a new method for DEM model calibration and ballast rheology study.

2. Methodology

2.1. Experimental test

2.1.1. Materials

The ballast particles utilised in the SSPT are crushed rocks of volcanic basalt, obtained from Tangshan Quarry, Hebei Province. Ballast material properties were confirmed based on the requirement in the British standard, i.e. the durability, mineralogy and particle morphology (shape, size) [40]. The ballast material properties are shown in Table 1. After testing, the ballast material meets the requirements in the standard thus it is suitable to be used as railway ballast. According to the British standard, ballast particles were sieved to reach the demanded particle size distribution (PSD, Grade A) [40]. The utilised sleeper is Chinese mono-block sleeper (750 kg) as shown in Figure 1. This sleeper type is the most common one in Chinese railways.

Table 1 Ballast material properties obtained from Tangshan Quarry (reproduced from [41]; same ballast material)

Property	Standard	Result	Maximum specification value
Micro-Deval loss (%)	BS EN 1097-1	5.20	7.00
Flakiness index (%)	BS EN 93-3	2.20	35.00
Elongation index (%)	BS EN 93-3	0.90	4.00
Fine particle content (%)	BS EN 933-1	0.30	0.60
Fines content (%)	BS EN 93-3	0.20	0.50

2.1.2. Test configuration and procedure

Figure 1 describes the track model (for the SSPT) configurations and the instrument setup positions. The track model for the SSPT was built by filling in a container with ballast particles and a sleeper. The ballast bed size meets the requirement of Chinses high speed railway design code [42], as shown in Figure 1a. The shoulder ballast width is 500 mm, the ballast thickness is 350 mm and the slope is 1: 1.75. Particularly, as shown in Figure 1b, one side of the container is made of glass to take photo of ballast assembly for analysing the ballast particle movements under the surface.

Two cameras were placed above and in front of the ballast bed, respectively. The camera above the track model was used to photograph the ballast shoulder, while the camera in front of the track model was used to photograph the cross section of the ballast bed.

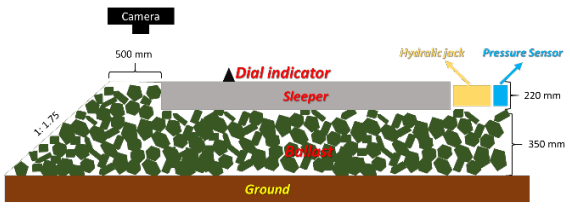

a. Front view of track model

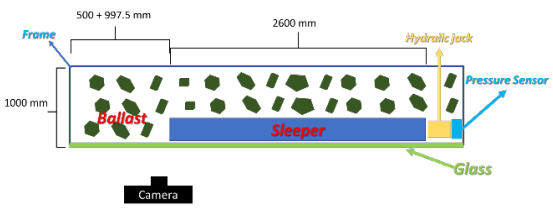

b. Top view of track model

c. Track model for single sleeper push test

Figure 1 Test configuration and instrument setup

A hydraulic jack and a pressure sensor were besides one side of the sleeper to push the sleeper and measure pushing force, respectively. A dial indicator was placed above the sleeper at the rail ditch to measure the sleeper displacement. The data acquisition system was connected to the pressure sensor to collect pushing force results. Table 2 presents the applied instruments and their parameters. The instruments include the pressure sensor, dial indicator, data acquisition system and hydraulic jack.

Table 2 Instruments and parameters (reproduced from [41]; same instruments)

Instrument name	Parameters
Hydraulic jack	Maximum loading: 10 ton; Actuator stroke: 10 cm
Data acquisition system	Name: IMC; Product model: INV3018A
Dial indicator	Precision 0.001 mm; measuring range 0~30 mm
Pressure sensor	Measuring range: 0~10 ton

After the materials and instruments are ready, the single sleeper push test procedure is described as follows:

1. Fill in the container with ballast particles at 350 mm thickness, and place the sleeper on the ballast bed next to the glass.
2. Fill in the ballast shoulder and the crib, and install all the instruments (Figure 1).
3. Start all the cameras, note that two more cameras were used to video the forces (data acquisition system) and the displacements (dial indicator) at the same time. This can obtain the force, displacement and ballast particle movements at the same time.
4. Push the sleeper and process the four videos, including ballast movements of shoulder, ballast movements of cross section, pushing forces and sleeper displacements.

2.1.3. Particle image velocimetry

The particle image velocimetry (PIV) is a method to process the digital image to measure the displacements of ballast particles by comparing two consecutively-taken photos. The PIV is to measure movements by observing the location changes of the target object in two or more images, as shown in Figure 2 [43].

Figure 2 presents the vertical displacements of the ballast particle at ballast shoulder. The displacements of ballast particles are calculated by comparing the initial image (initial stage) with the following images (ballast particles moved), and this calculation is dependent on the movements of the pixels. By defining a pixel presents a certain actual distance, the ballast particle displacements can be measured from the pixel displacements through image comparison.

The horizontal and vertical displacements of ballast particles are defined as the vertical and horizontal directions in the figure, which is marked in Figure 2. All the results are presented respectively by horizontal and vertical displacements in the following sections. Using this means to present ballast

particle displacements is easy to compare the displacement results to DEM results. The colour labels in the right side of each figures are the values of particle displacements.

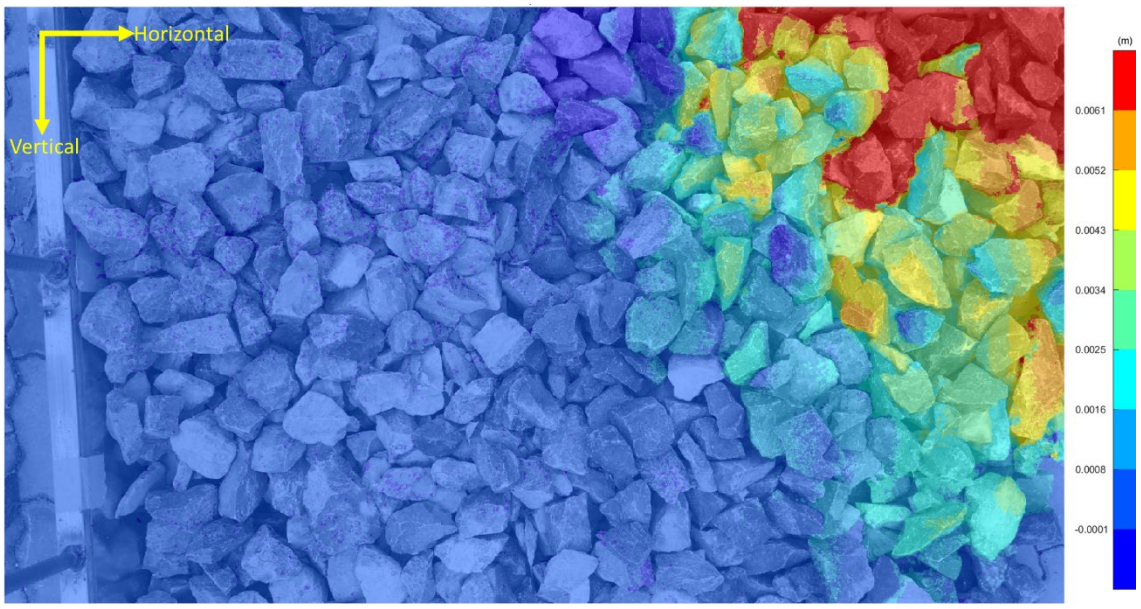

a. Ballast particle displacements at ballast shoulder

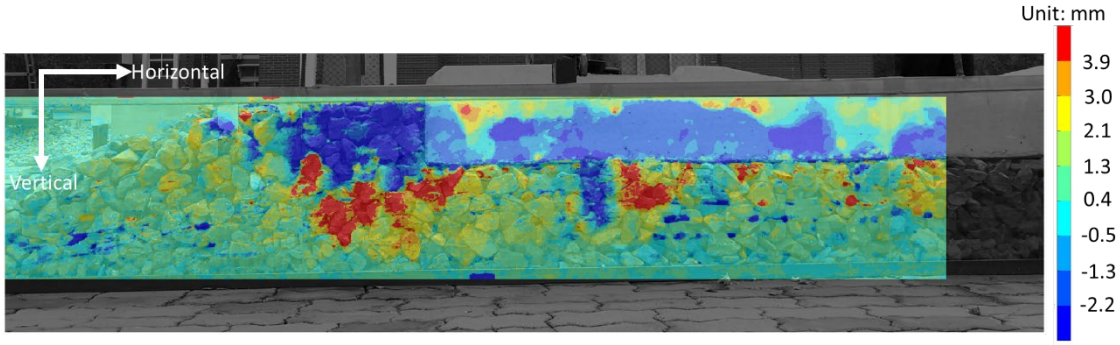

b. Ballast particle displacements at cross section of ballast bed

Figure 2 Calculation methods for displacement

2.2. Discrete element modelling

The commercial DEM software utilised in this study is particle flow code in three-dimensional (PFC3D). There are two basic elements in PFC3D, spheres and walls, and the Newton's second law is applied for the force-displacement cycles of all the spheres [27]. With the PFC3D, the numerical model (single sleeper push test) is built according to the test configuration, as shown in Figure 3a.

The sleeper is modelled with walls according to the real sleeper configuration. Specifically, the mono-block sleeper was drawn in AutoCAD, and then exported as "stl" format. Afterwards, the sleeper drawing was imported in the PFC3D, and based on the drawing the modelled sleeper is generated as shown in Figure 3b.

Figure 3c presents a method to create ballast particles using 3D ballast particle image. Firstly, 3D ballast images were obtained from laser scanning, and the "stl" format ballast images were imported in the PFC3D as geometries. Afterwards, spheres with overlaps were filled in one geometry to present one ballast particle. More spheres for one ballast particle contribute to more precise particle, and Figure 3d presents some examples of applied particles.

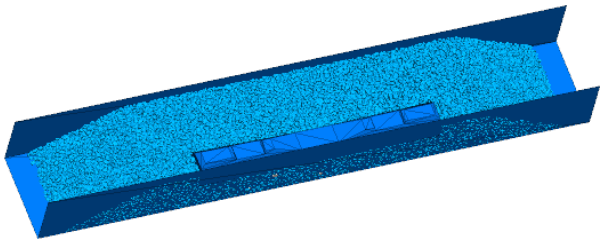

a. DEM single-sleeper track model

b. Sleeper generation

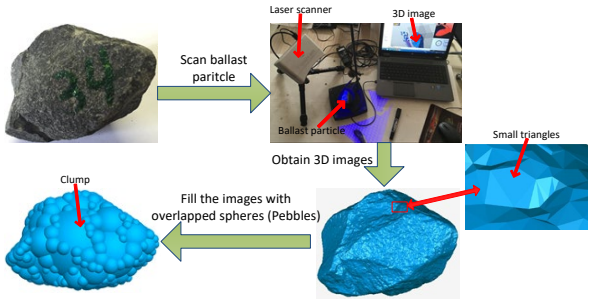

c. Ballast particle generation (reproduced from [43])

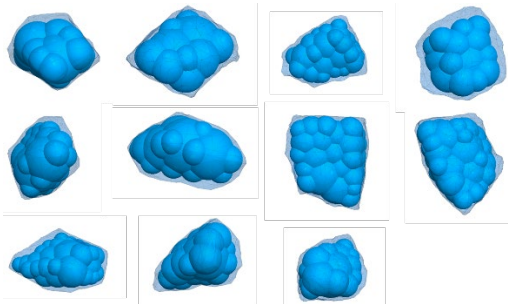

d. Ballast particle model library

Figure 3 Single sleeper push test model and model details

The parameters that are applied in the model for calibration are given in Table 3, including the friction and stiffness for the contact model (linear contact model) at every contact including, particle-particle contacts, particle-sleeper contacts and particle-glass contacts.

Table 3 Parameters for PFC3D model calibration

Component	Parameter	Value
Ballast	Density	2700
	Friction	0.55
	Shear stiffness	5×10^9
	Normal stiffness	2×10^9
Sleeper	Friction	0.55
	Shear stiffness	1×10^9
	Normal stiffness	1×10^9
Glass wall	Friction	0.5
	Shear stiffness	5×10^9
	Normal stiffness	5×10^9

3. Results and discussions

3.1. Lateral resistance

As shown in Figure 4, the experimental and numerical results of lateral resistance are presented and compared. The figure demonstrates that the results from experiment or numerical simulation are matched with low differences.

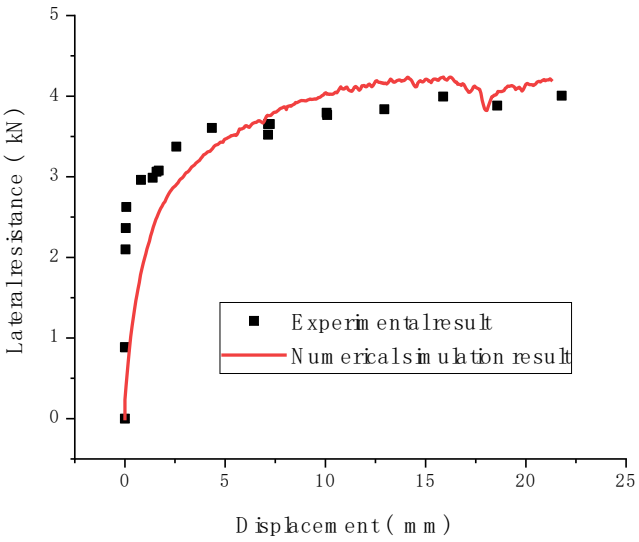

Figure 4 Lateral resistance vs. displacement of single sleeper push test

Figure 4 shows the peak value of the lateral resistance (both experimental and numerical) is lower than normal value (usually, around 10 kN). This is due to no ballast particles were placed at one side of the sleeper (glass wall side), as shown in Figure 1b. In addition, the ballast beds (both experimental and numerical) are not fully compacted, which is another reason to the low lateral resistance value.

In the following sections, the particle displacements of the SSPTs are mainly focused (both experimental and numerical), and the displacement results of PIV or DEM simulation are compared. The comparison of the particle displacement results is meaningful. Because in most earlier studies, the statements are similar to the following, "since these two curves (Figure 4) are matched, this DEM model is correct and validated and can be used for other analysis". However, the parameters in these validated models, such as, parameters of the applied contact model: normal stiffness and shear stiffness, are not suitable for other kinds of models, which means these parameters could only be used for the current validated models. This was demonstrated in some studies, e.g., [31, 44].

3.2. Ballast rheology from PIV results

The ballast rheology from PIV results is presented by ballast particle displacements at different sleeper displacements. The sleeper displacements were from the scatter points of experimental lateral resistance results (Figure 4). All the ballast rheology results are given in tables (Appendix), including

- horizontal displacements of ballast particles at ballast bed cross section (Table A. 1),
- vertical displacements of ballast particles at ballast bed cross section (Table A. 2),
- horizontal displacements of ballast particles at ballast shoulder (Table A. 3),
- and vertical displacements of ballast particles at ballast shoulder (Table A. 4).

3.2.1. Horizontal displacements of ballast particles at ballast bed cross section

According to the Table A. 1, the ballast particle rheology is analysed in this section (at horizontal direction). Figure 5 presents the horizontal displacements of ballast particles (ballast bed cross section) at four different sleeper displacements, i.e., 0.002, 7.142, 10.089 and 21.789 mm, which are selected from Table A. 1. In the figure, the SD is short for sleeper displacement, and the LR is short for lateral resistance. From Figure 5, ballast particle displacements are observed and analysed.

Figure 5a is the initial stage of the SSPT, which means at that moment it was just started to push the sleeper. The figure shows at the initial stage the lateral resistance has already reached a big value 25% of the peak value, but the ballast particles have very few displacements. This is possibly due to the

inertia of sleeper and ballast assemblies. When a train was running on a track, the impact lateral forces were normally excreted to the track, and the impact forces mostly are dissipated by the inertia of sleeper and ballast assemblies. That means high lateral resistance at the initial stage is needed for the consideration of ride safety and comfort.

Figure 5b presents the ballast particle displacements as the sleeper displacement was at 7.142 mm. This figure was chosen to study ballast rheology, because the sleeper displacement at 7.142 mm almost reached the peak resistance value. The figure shows that the ballast particles next to the sleeper end have the largest displacements, and ballast particles near the sleeper end have smaller and smaller displacements as their distances to sleeper increases. This demonstrates that ballast particles are condensed (densification) to resist the forces from the sleeper.

The ballast particles that have large displacements (in blue) make a quadrangle, which is marked in the Figure 5b. The deepest ballast particles that have displacements are under the sleeper with around 20.8 cm distances, and 36 degrees are the internal friction angle. The two values are possibly different at different compaction degrees of ballast beds.

In some areas of Figure 5b, the ballast particles have positive displacements (in red). The positive displacements are very small with value normally smaller than 2 mm. This is due to at these areas the ballast particles have poor contact with the sleeper, and ballast particles have not only translation movements but also rotations.

In the area under the sleeper of Figure 5b, the ballast particles have big displacements (in cyan). These areas have big ballast displacements, because the ballast particles have good contacts with the sleeper. The good sleeper-ballast contacts increase the ballast particle numbers that contribute to the lateral resistance, additionally, deeper ballast particles contribute to the lateral resistance.

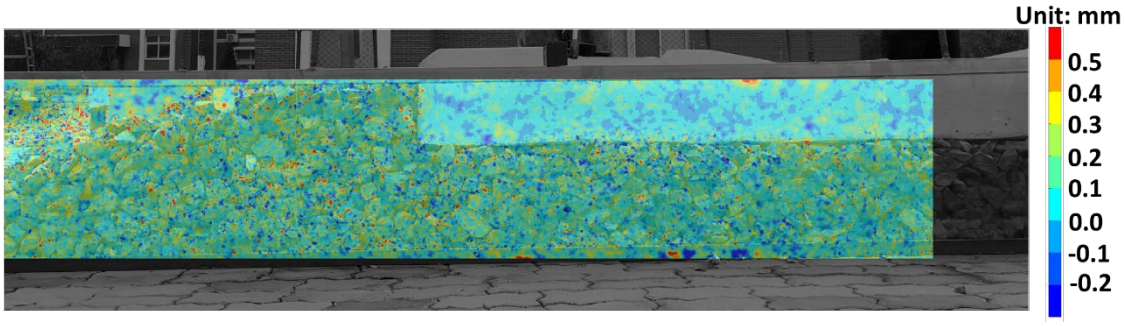

a. SD: 0.002 mm; LR: 0.8855 kN

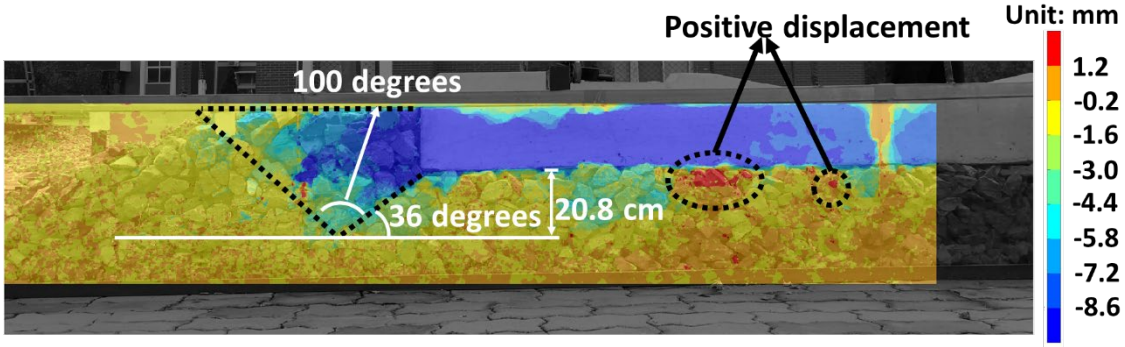

b. SD: 7.142 mm; LR: 3.522 kN

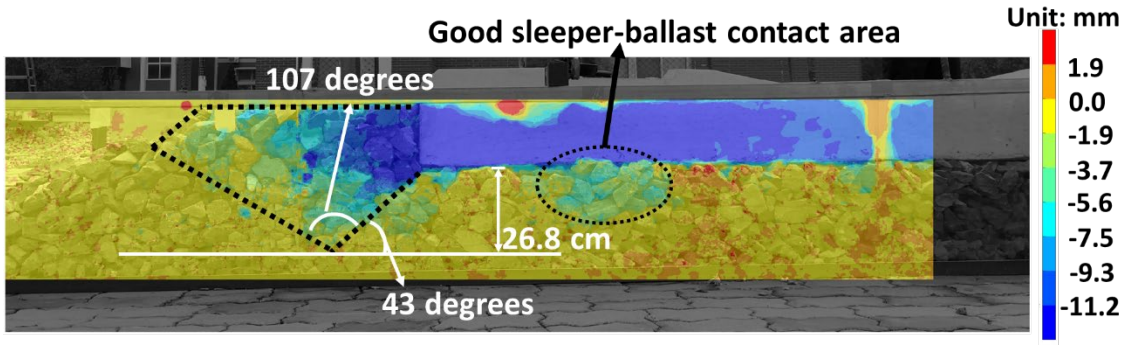

c. SD: 10.089 mm; LR: 3.766 kN

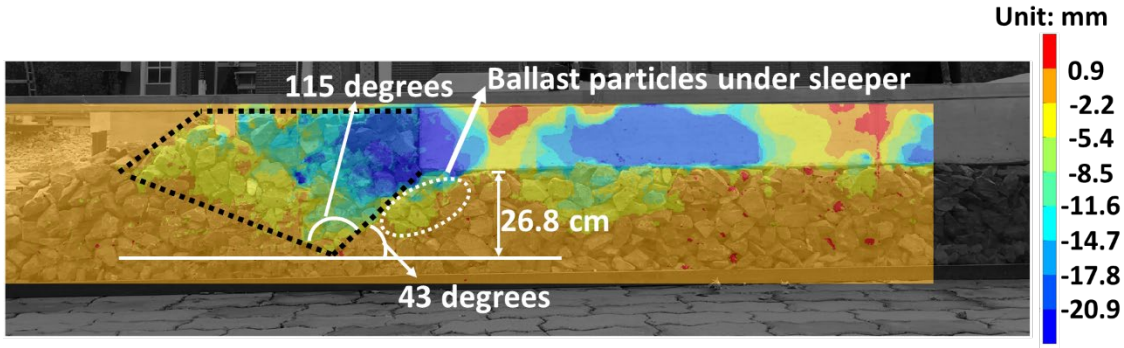

d. SD: 21.789 mm; LR: 4.005 kN

Figure 5 Horizontal displacements of ballast particles at ballast bed cross section

Figure 5c presents the ballast particle displacements as the sleeper displacement was 10.089 mm, which was in a stable stage of the lateral resistances. It shows that the ballast particles with big displacements increase, which is presented by larger internal friction angle (43°) and deeper distance under the sleeper (23 cm) of the ballast particles. By comparing Figure 5c to Figure 5b, the ballast particles under the sleeper that provide the resistance (in cyan) are almost at the same position but with larger ballast particle displacements.

Figure 5d shows the ballast particle displacements as the sleeper displacement was 21.789 mm, which was the final stage of the SSPT. It shows that the ballast particles with big displacements increased, but the internal friction angle and distance under the sleeper of ballast particles are not changed, 43° and 26.8 cm, respectively. As the marked in a circle (Figure 5d), the ballast particles under the sleeper also have big displacements, which is due to 1) the good sleeper-ballast contacts and 2) the sleeper pushed the ballast away making a slope and the ballast particles slid from the slope.

3.2.2. Vertical displacements of ballast particles at ballast bed cross section

According to the Table A. 2, the ballast particle rheology is analysed in this section (at vertical direction). Figure 6 presents the vertical displacements of ballast particles in ballast bed cross section at four different sleeper displacements, i.e., 0.002, 7.142, 10.089 and 21.789 mm, which are selected from Table A. 2. From Figure 6, ballast rheology is observed and analysed based on ballast particle displacements.

Figure 6a presents the initial stage of the SSPT, when it was just started to push the sleeper (0.002 mm). The figure shows at the initial stage the lateral resistance has already reached a big value 25% of the peak value, but the ballast particles have very few vertical displacements. The reason of this phenomenon was discussed in Section 3.2.1.

Figure 6b presents the vertical displacements of ballast particle as the sleeper displacement was at 7.142 mm. The figure shows that the largest displacements appear around the sleeper end, including both the negative and positive displacements. As shown in Figure 6b, the largest negative

displacements of ballast particles (in blue) are marked in a square, and the largest positive displacements of ballast particles (in red) are marked in a triangle. This demonstrates the sleeper end pushed the ballast particles either go up (negative displacement) or go down (positive displacement), which are separated by the sleeper bottom line. The shoulder ballast particles usually go up, and the ballast particle under the sleeper bottom line go down.

Note that some particles in the square (in green) have small negative displacements, which is due to squeezing the ballast particles at the shoulder makes some particles slightly go down. In addition, higher positive displacement values (3.3 mm) were found during the SSPT than negative displacement values (-0.5 mm). Particularly, a big positive area is usually next a big negative area, as shown in Figure 6b (in the circle). This means the ballast particles are pushed going down, which also causes lifting up the nearby ballast particles.

The ballast particles under the sleeper that have big positive vertical displacements in Figure 6b also show big horizontal displacements in Figure 5b, which proves the discussion of good contacts between sleeper and ballast is correct (in Section 3.2.1).

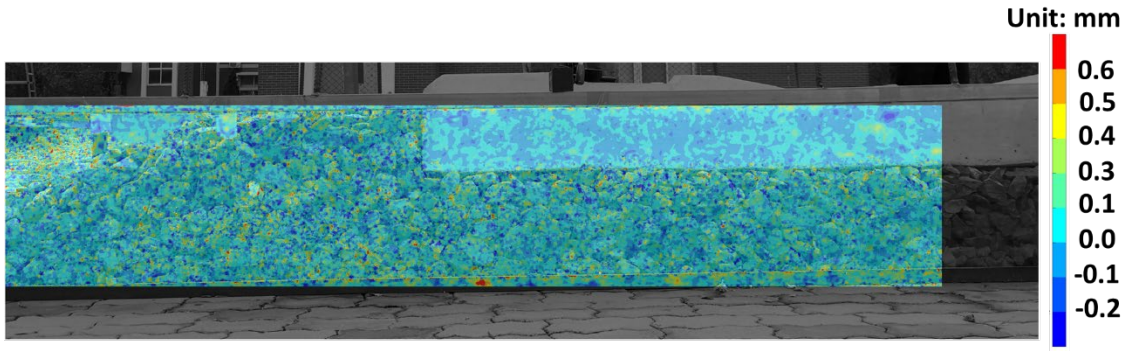

a. SD: 0.002 mm; LR: 0.8855 kN

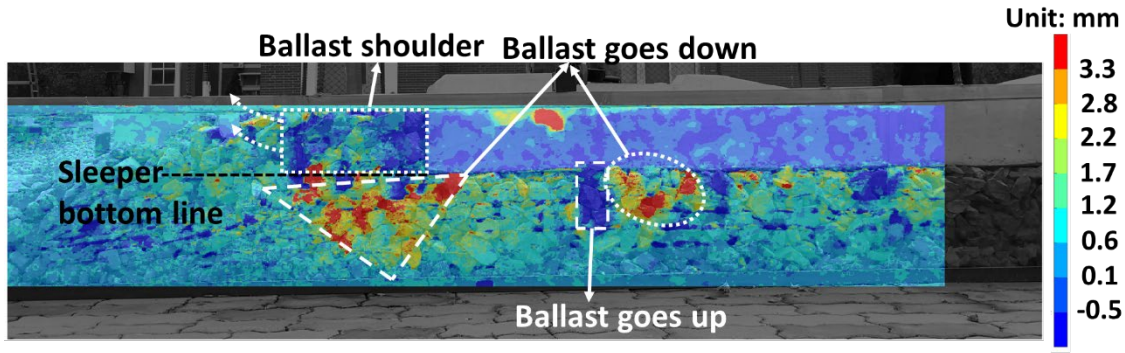

b. SD: 7.142 mm; LR: 3.522 kN

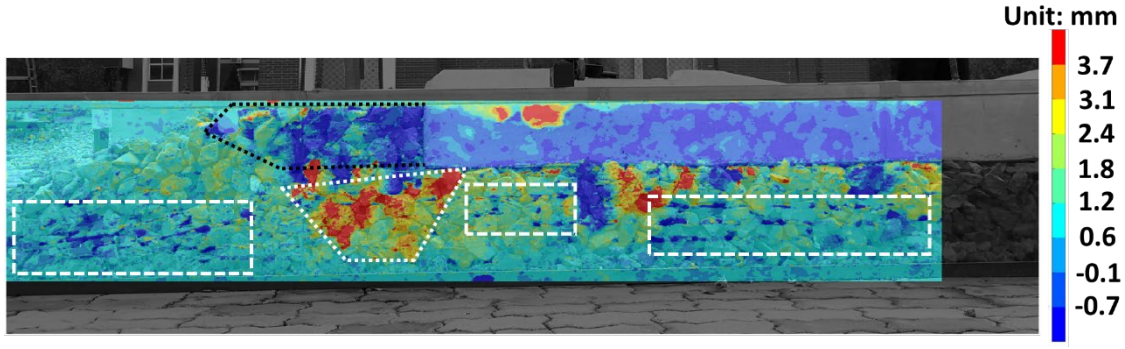

c. SD: 10.089 mm; LR: 3.766 kN

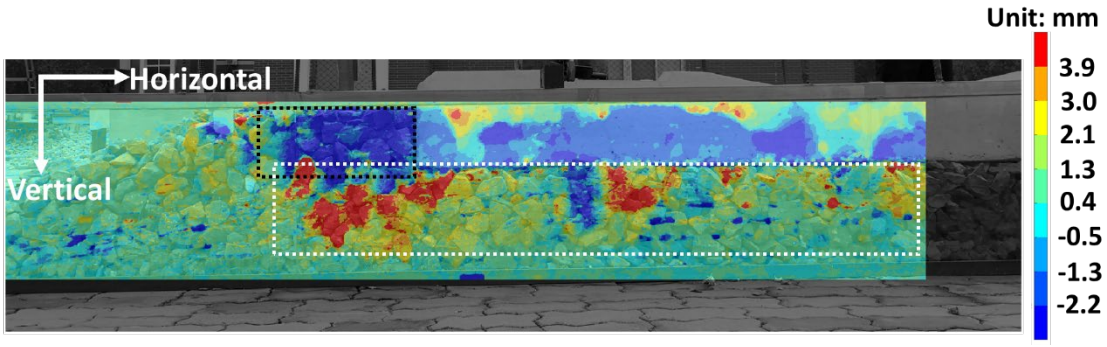

d. SD: 21.789 mm; LR: 4.005 kN

Figure 6 Vertical displacements of ballast particles at ballast bed cross section

Figure 6c presents the ballast particle vertical displacements as the sleeper displacement was 10.089 mm, which was in a stable stage of the lateral resistances. The figure shows the negative displacements of ballast particles at the ballast shoulder slightly become bigger from -0.5 mm to -0.7 mm, and the positive ballast displacements under the sleeper bottom line slightly increased from 3.3 mm to 3.7 mm. however, the sizes of the areas with big ballast displacements almost remain the same.

Interestingly, the ballast particles marked in rectangles have the wave shape, which is more clearly observed at small sleeper displacements from 0.046 mm to 1.582 mm (Table A. 2). This is possibly due to the ballast particles have small rotations, and the small rotations result from that the ballast bed is not adequately compacted.

Figure 6d shows the vertical displacements ballast particle as the sleeper displacement was 21.789 mm, which was the final stage of the SSPT. The figure shows almost all the ballast particles under the sleeper go down (positive displacements), except the ballast particle in one area (in blue) with negative displacements around 2.2 mm. Almost all the ballast particles that go up (with negative displacements) are at the position of ballast shoulder, which is marked in black rectangle in Figure 6d.

3.2.3. Horizontal displacements of ballast particles at ballast shoulder

According to the Table A. 3, the ballast particle rheology is analysed in this section (at horizontal direction). Figure 7 presents the horizontal displacements of ballast particles in ballast shoulder at four different sleeper displacements, i.e., 0.002, 7.142, 10.089 and 21.789 mm, which are selected from Table A. 3. From Figure 7, ballast rheology is observed and analysed based on ballast particle displacements.

Figure 7a presents the initial stage of the SSPT, when it was just started to push the sleeper (0.002 mm). The figure shows at the initial stage the lateral resistance has already reached a big value 25% of the peak value, but the ballast particles have almost no movements. The reason of this phenomenon was discussed in Section 3.2.1.

Figure 7b presents the horizontal displacements of ballast particle as the sleeper displacement was at 7.142 mm. The figure demonstrates that the largest ballast horizontal displacements are around the sleeper end, including both the negative and positive displacements. Big negative displacements of ballast particles (in blue) are at right side of the sleeper, and big positive displacements (in red) are at the left side of the sleeper. This means that the sleeper end pushed the ballast particles either go left (negative displacement) or go right (positive displacement). Particularly, the ballast displacements are small at horizontal direction, which is due to the ballast particles mainly move at same direction as sleeper displacement (vertical direction in Figure 7).

Figure 7c presents the ballast particle horizontal displacements as the sleeper displacement was 10.089 mm, which was in a stable stage of the lateral resistances. The figure shows the ballast particle

displacements have small increase, compared with Figure 7b: 1) positive displacements from 0.7 mm to 1.6 mm, and positive displacements mean that ballast particles move to right side; 2) and negative displacements from -0.2 mm to -0.4 mm, and negative displacements mean that ballast particles move to left side.

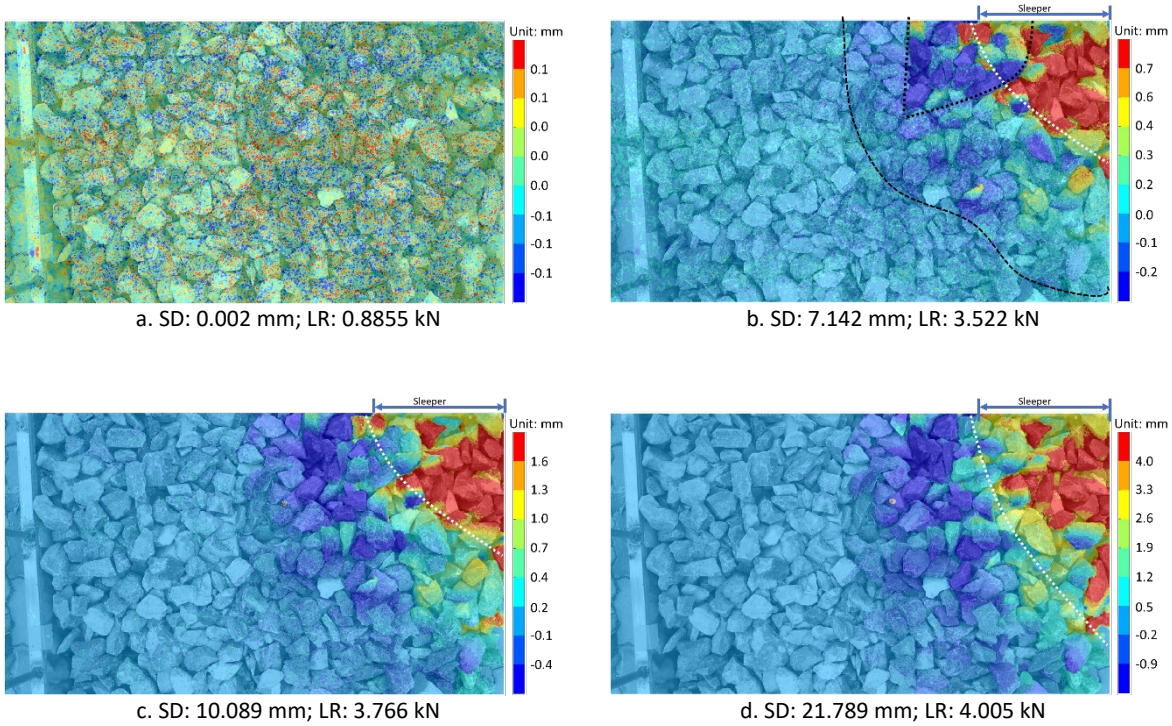

a. SD: 0.002 mm; LR: 0.8855 kN

b. SD: 7.142 mm; LR: 3.522 kN

c. SD: 10.089 mm; LR: 3.766 kN

d. SD: 21.789 mm; LR: 4.005 kN

Figure 7 Horizontal displacements of ballast particles at ballast shoulder

Figure 7d shows the horizontal displacements ballast particle as the sleeper displacement was 21.789 mm, which was the final stage of the SSPT. The figure shows that the maximum horizontal displacements of ballast particles are 4.0 mm, which is not very big possibly because of the restriction of the glass wall next to the sleeper (Figure 1b). Ballast particles have very small displacements to the left side (maximum 0.9 mm), even though there are no restrictions.

3.2.4. Vertical displacements of ballast particles at ballast shoulder

According to the Table A. 4, the ballast particle rheology is analysed in this section (at vertical direction). Figure 8 presents the vertical displacements of ballast particles in ballast shoulder at four different sleeper displacements, i.e., 0.002, 7.142, 10.089 and 21.789 mm, which are selected from Table A. 4. Based on Figure 8, ballast rheology is observed and analysed based on ballast particle displacements.

Figure 8a presents the initial stage of the SSPT, when it was just started to push the sleeper (0.002 mm). Similar to the other former initial figures, the ballast particles have almost no movements.

Figure 8 b/c/d summarise the ballast particle vertical displacements under three conditions with different sleeper displacements. The figures show that the ballast particles near the sleeper end have bigger displacements as expected. In addition, the maximum particle displacements increase as the sleeper displacement increases. Particularly, the maximum ballast particle displacement at the ballast shoulder is 6.1 mm as the sleeper displacement was 21.789 mm (Figure 8d), which means the ballast particles at the shoulder have big rotations instead of translation movements. Even so, almost all the ballast particles at the ballast shoulder (50 cm shoulder width) have displacements as the sleeper displacement was 21.789 mm.

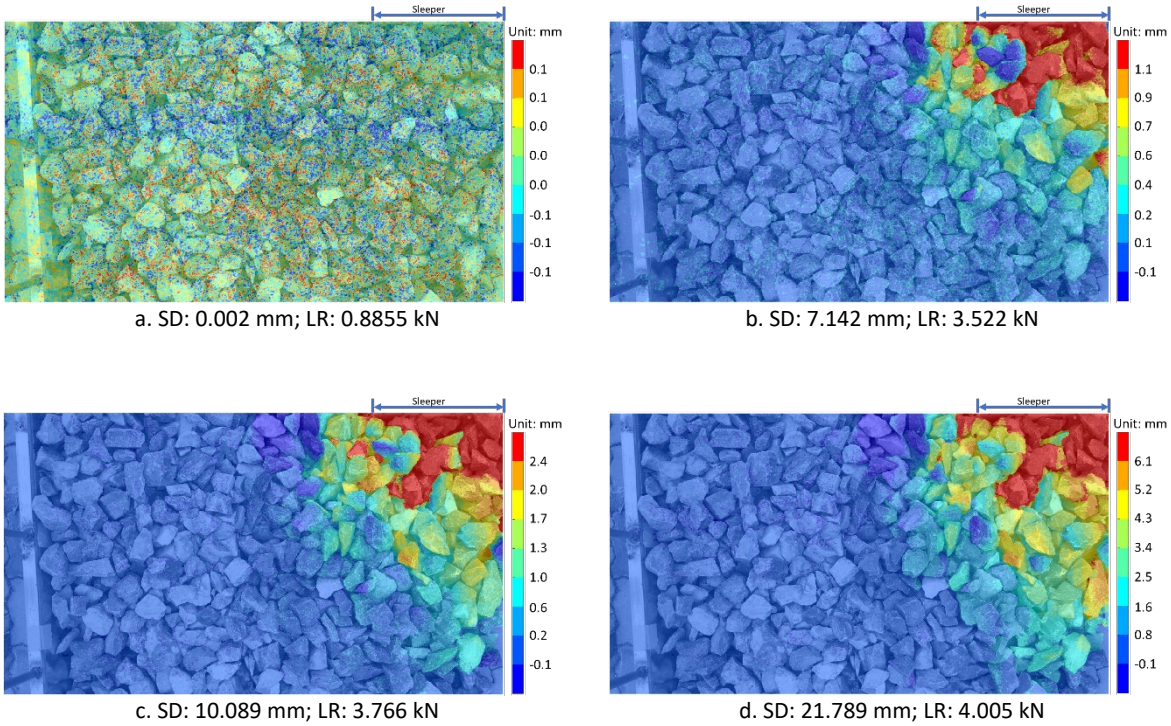

a. SD: 0.002 mm; LR: 0.8855 kN

b. SD: 7.142 mm; LR: 3.522 kN

c. SD: 10.089 mm; LR: 3.766 kN

d. SD: 21.789 mm; LR: 4.005 kN

Figure 8 Vertical displacements of ballast particles at ballast shoulder

3.3. Ballast rheology comparison between DEM and PIV results

In this section, the ballast rheology compassion between DEM and PIV results is performed by comparing the ballast particle displacements. The ballast particle displacement results of four different sleeper displacements are shown in Table A. 5 (0.002 mm), Table A. 6 (10.089 mm), Table A. 7 (21.789) and Figure 9 (7.142 mm), respectively. The ballast particle displacement comparison of DEM and PIV at 7.142 mm sleeper displacement (Figure 9) is explained and discussed as an example. As shown in Figure 9, their colour ranges (maximum and minimum value) are set the same to more easily compare the displacements.

As shown in Figure 9 a/b, the ballast particle displacements at the ballast shoulder are acceptable matched. For example, the ballast particles next to the sleeper end have the biggest displacements, and the big displacements areas (DEM results or PIV results) are the same shape. A few ballast particles under the sleeper have positive displacements. The Failure angles are the same at 36 degrees. However, the deepest ballast particles below the sleeper that have big displacements have different depths, 16.2 cm and 20.8 cm, respectively. This difference is possibly due to the ballast bed was not sufficiently compacted and some ballast particles have weak contacts with nearby particles, then the ballast particles started to drop and slide. Nevertheless, the overall ballast motion modes (DEM or PIV) are similar, and the small result differences can be eliminated by improving the test conditions, facility precesion and DEM model parameters.

Similarly, as shown in Figure 9 c/d, the overall ballast motion modes (DEM or PIV) also show similar to each other. To be more specific, ballast displacement directions (up or down) at sleeper end are separated by the sleeper bottom line, and under the sleeper at some locations, the two areas that ballast particles have opposite displacement directions (Figure 9 c in the circle) are next to each other. Particularly, the ballast particles at the sleeper end of going down (DEM or PIV) are different at total particle numbers, in other words, the ballast particles at sleeper end (in DEM) are less likely to go down than in PIV. This demonstrates the hypothesis in last paragraph about weak particle contacts and big particle dropping and sliding displacements of PIV results.

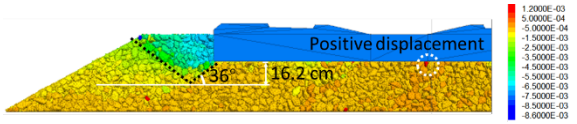

a. Horizontal displacements of ballast particles ballast bed cross section (DEM)

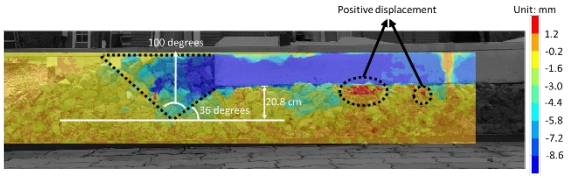

b. Horizontal displacements of ballast particles at ballast bed cross section (PIV)

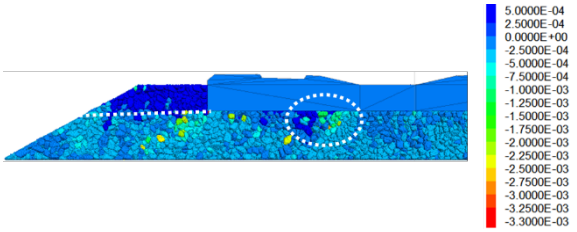

c. Vertical displacements of ballast particles ballast bed cross section (DEM)

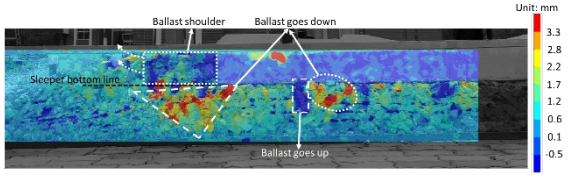

d. Vertical displacements of ballast particles at ballast bed cross section (PIV)

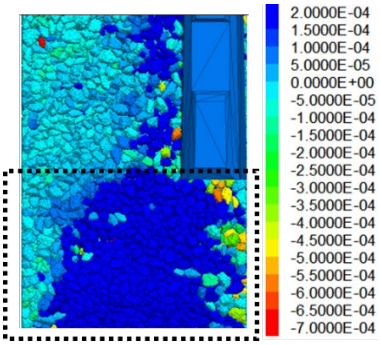

e. Horizontal displacements of ballast particles at ballast shoulder (DEM)

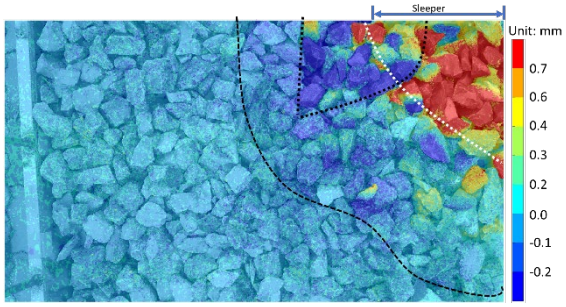

f. Horizontal displacements of ballast particles at ballast shoulder (PIV)

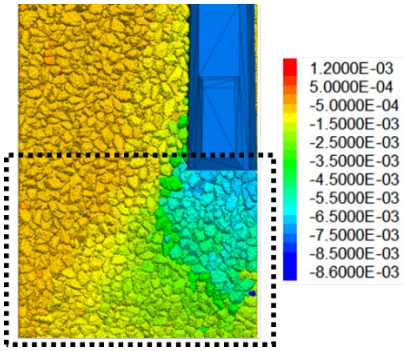

g. Vertical displacements of ballast particles at ballast shoulder (DEM)

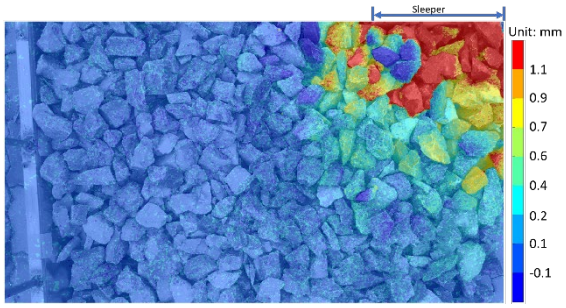

h. Vertical displacements of ballast particles at ballast shoulder (PIV)

Figure 9 Comparison of ballast particle displacement results from DEM or PIV with 7.142 mm sleeper displacement

As shown in Figure 9 e/f/g/h, DEM and PIV results of ballast particles at the ballast shoulder surface are compared. The figures show that the ballast motion modes (DEM or PIV) are similar, but their values are with big difference. This is due to at the ballast shoulder ballast particles have big rotations during the experimental SSPT, and especially the ballast particles at the ballast shoulder surface have much less contacts than inside of the ballast bed. Big ballast particle rotations cause the ballast image changed very fast, and some pixels are missing and cannot be compared to the former images to calculate displacements, which leads to big errors. This phenomenon was not observed in the ballast bed cross section, because the ballast particles were contacted with the glass wall.

From the comparisons and discussions, it demonstrates that using ballast particle displacements from PIV is possible to calibrate and validate DEM models. It also reflects that the earlier “force-displacement calibration method” can be used combined with the PIV calibration method, which leads

to more accurate and correct DEM model. Most importantly, the PIV technique still needs improvement to detect particle rotation, which can better be used to calibrate and validate DEM models.

4. Conclusions

This paper proposed a method using Particle Image Velocimetry (PIV) to study ballast rheology, and also to calibrate and validate discrete element method (DEM) model. To demonstrate the method feasibility, the single sleeper push test was performed both with PIV and with DEM to obtain ballast particle displacements. By studying and comparing the ballast particle displacements (from DEM or PIV), the following conclusions are given.

1. The lateral resistance from sleeper bottom is significantly influenced by the contacts between ballast and sleeper. In addition, ballast particles at sleeper bottom in most cases have very small displacements.
2. The peak lateral resistance is reached as ballast particles (at the ballast shoulder next sleeper end) are fully condensed.
3. It is feasible to use the PIV for DEM model calibration and validation, and this method is a good additional means to improve the calibration and validation accuracy instead of only using the macro mechanical results (e.g., force-displacement curve).

5. Acknowledgements

The research is supported by the Natural Science Foundation of China (Grant No.51578051). The image analysis was performed by Zhilei Luo under the guidance of Prof. Linlin Wang (China University of Petroleum), for which we would like to show our great appreciation.

6. References

[1] H. Liu, J. Xiao, P. Wang, G. Liu, M. Gao, S. Li, Experimental investigation of the characteristics of a granular ballast bed under cyclic longitudinal loading, Construction and Building Materials 163 (2018) 214-224.
[2] Y. Guo, V. Markine, X. Zhang, W. Qiang, G. Jing, Image analysis for morphology, rheology and degradation study of railway ballast: A review, Transportation Geotechnics 18 (2019) 173-211.
[3] J. Xiao, D. Zhang, K. Wei, Z. Luo, Shakedown behaviors of railway ballast under cyclic loading, Construction and Building Materials 155 (2017) 1206-1214.
[4] J. Liu, P. Wang, G. Liu, J. Xiao, H. Liu, T. Gao, Influence of a tamping operation on the vibrational characteristics and resistance-evolution law of a ballast bed, Construction and Building Materials 239 (2020) 117879.
[5] J. Liu, P. Wang, G. Liu, M. Zhang, J. Xiao, H. Liu, Uniaxial compression characteristics of railway ballast combined with ice, Construction and Building Materials 263 (2020).
[6] J. Liu, P. Wang, G. Liu, J. Dai, J. Xiao, H. Liu, Study of the characteristics of ballast bed resistance for different temperature and humidity conditions, Construction and Building Materials 266 (2021).
[7] F. Khatibi, M. Esmaeili, S. Mohammadzadeh, Numerical investigation into the effect of ballast properties on buckling of continuously welded rail (CWR), Proceedings of the Institution of Mechanical Engineers, Part F: Journal of Rail and Rapid Transit (2020).
[8] J. Ali Zakeri, M. Esmaeili, A. Kasraei, A. Bakhtiary, A numerical investigation on the lateral resistance of frictional sleepers in ballasted railway tracks, Proceedings of the Institution of Mechanical Engineers, Part F: Journal of Rail and Rapid Transit 230(2) (2014) 440-449.
[9] S. Liu, H. Huang, T. Qiu, B. Kerchof, Characterization of Ballast Particle Movement at Mud Spot, Journal of Materials in Civil Engineering 31(1) (2018) 04018339.
[10] D. Li, J. Hyslip, T. Sussmann, S. Chrismer, Railway geotechnics, CRC Press2002.
[11] M. Esmaeili, K. Yousefian, R. Nouri, Vertical load distribution in ballasted railway tracks with steel slag and limestone ballasts, International Journal of Pavement Engineering (2017) 1-8.
[12] J.A. Zakeri, R. Abbasi, Field investigation on variation of rail support modulus in ballasted railway tracks, Lat Am J Solids Stru 9(6) (2012) 643-656.
[13] A. Bakhtiary, J.A. Zakeri, S. Mohammadzadeh, An opportunistic preventive maintenance policy for tamping scheduling of railway tracks, International Journal of Rail Transportation (2020) 1-22.
[14] Y. Qian, S.J. Lee, E. Tutumluer, Y.M.A. Hashash, J. Ghaboussi, Role of Initial Particle Arrangement in Ballast Mechanical Behavior, International Journal of Geomechanics 18(3) (2018) 04017158.

[15] L. Le Pen, A.R. Bhandari, W. Powrie, Sleeper End Resistance of Ballasted Railway Tracks, Journal of Geotechnical and Geoenvironmental Engineering 140(5) (2014) 04014004.
[16] C. Shi, C. Zhao, X. Zhang, Y. Guo, Coupled discrete-continuum approach for railway ballast track and subgrade macro-meso analysis, International Journal of Pavement Engineering (2020) 1-16.
[17] N.T. Ngo, B. Indraratna, C. Rujikiatkamjorn, Simulation Ballasted Track Behavior: Numerical Treatment and Field Application, International Journal of Geomechanics 17(6) (2016) 04016130.
[18] J. Harkness, A. Zervos, L. Le Pen, S. Aingaran, W. Powrie, Discrete element simulation of railway ballast: modelling cell pressure effects in triaxial tests, Granular Matter 18(3) (2016) 1-13.
[19] C. Chen, B. Indraratna, G. McDowell, C. Rujikiatkamjorn, Discrete element modelling of lateral displacement of a granular assembly under cyclic loading, Computers and Geotechnics 69 (2015) 474-484.
[20] B. Indraratna, T. Ngo, Ballast railroad design: smart-uow approach, CRC Press2018.
[21] S. Liu, T. Qiu, Y. Qian, H. Huang, E. Tutumluer, S. Shen, Simulations of large-scale triaxial shear tests on ballast aggregates using sensing mechanism and real-time (SMART) computing, Computers and Geotechnics 110 (2019) 184-198.
[22] G. Jing, H. Fu, P. Aela, Lateral displacement of different types of steel sleepers on ballasted track, Construction and Building Materials 186 (2018) 1268-1275.
[23] Y. Qian, D. Mishra, E. Tutumluer, H.A. Kazmee, Characterization of geogrid reinforced ballast behavior at different levels of degradation through triaxial shear strength test and discrete element modeling, Geotextiles and Geomembranes 43(5) (2015) 393-402.
[24] X. Zhang, C. Zhao, W. Zhai, DEM Analysis of Ballast Breakage Under Train Loads and Its Effect on Mechanical Behaviour of Railway Track, Proceedings of the 7th International Conference on Discrete Element Methods 188 (2017) 1323-1333.
[25] J. de Bono, H. Li, G. McDowell, A new abrasive wear model for railway ballast, Soils and Foundations 60(3) (2020) 714-721.
[26] C. Coetzee, Calibration of the discrete element method, Powder Technology 310 (2017) 104-142.
[27] Y. Guo, C. Zhao, V. Markine, G. Jing, W. Zhai, Calibration for discrete element modelling of railway ballast: A review, Transportation Geotechnics (2020) 100341.
[28] J. Irazábal, F. Salazar, E. Oñate, Numerical modelling of granular materials with spherical discrete particles and the bounded rolling friction model. Application to railway ballast, Computers and Geotechnics 85 (2017) 220-229.
[29] L. Li, W. Liu, M. Ma, G. Jing, W. Liu, Research on the dynamic behaviour of the railway ballast assembly subject to the low loading condition based on a tridimensional DEM-FDM coupled approach, Construction and Building Materials 218 (2019) 135-149.
[30] S. Lobo-Guerrero, L.E. Vallejo, L.F. Vesga, Visualization of crushing evolution in granular materials under compression using DEM, International Journal of Geomechanics 6(3) (2006) 195-200.
[31] Y. Guo, C. Zhao, V. Markine, C. Shi, G. Jing, W. Zhai, Discrete element modelling of railway ballast performance considering particle shape and rolling resistance, Railway Engineering Science (2020).
[32] Z. Wang, G. Jing, Q. Yu, H. Yin, Analysis of ballast direct shear tests by discrete element method under different normal stress, Measurement 63 (2015) 17-24.
[33] X. Bian, W. Li, Y. Qian, E. Tutumluer, Micromechanical Particle Interactions in Railway Ballast through DEM Simulations of Direct Shear Tests, International Journal of Geomechanics 19(5) (2019).
[34] N.T. Ngo, B. Indraratna, C. Rujikiatkamjorn, Modelling geogrid-reinforced railway ballast using the discrete element method, Transportation Geotechnics 8 (2016) 86-102.
[35] M. Lu, G.R. McDowell, Discrete element modelling of railway ballast under triaxial conditions, Geomechanics and Geoengineering 3(4) (2008) 257-270.
[36] X. Zhang, C. Zhao, W. Zhai, Dynamic Behavior Analysis of High-Speed Railway Ballast under Moving Vehicle Loads Using Discrete Element Method, International Journal of Geomechanics 17(7) (2016) 04016157.
[37] M. Esmaeili, A. Khodaverdian, H.K. Neyestanaki, S. Nazari, Investigating the effect of nailed sleepers on increasing the lateral resistance of ballasted track, Computers and Geotechnics 71 (2016) 1-11.
[38] M. Esmaeili, J.A. Zakeri, M. Babaei, Laboratory and field investigation of the effect of geogrid-reinforced ballast on railway track lateral resistance, Geotextiles and Geomembranes 45(2) (2017) 23-33.
[39] R. Takahashi, K. Hayano, T. Nakamura, Y. Momoya, Integrated risk of rail buckling in ballasted tracks at transition zones and its countermeasures, Soils and Foundations 59(2) (2019) 517-531.
[40] B.s.p.B.E. British Standards Institution, Aggregates for railway ballast, British Standards Institution London, 2013.
[41] Y. Guo, H. Fu, Y. Qian, V. Markine, G. Jing, Effect of sleeper bottom texture on lateral resistance with discrete element modelling, Construction and Building Materials 250 (2020).
[42] N.R.A.o.t.P.s.R.o. China, Code for design of high speed railway, TB 1062-2014 (2014).
[43] Y. Guo, V. Markine, W. Qiang, H. Zhang, G. Jing, Effects of crumb rubber size and percentage on degradation reduction of railway ballast, Construction and Building Materials 212 (2019) 210-224.
[44] B. Suhr, S. Marschnig, K. Six, Comparison of two different types of railway ballast in compression and direct shear tests: experimental results and DEM model validation, Granular matter 20(4) (2018) 70.

7. Appendix

Table A. 1 Horizontal displacements of ballast particles at ballast bed cross section (SD-sleeper displacement; LR-lateral resistance)

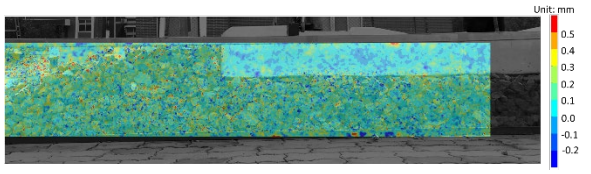 SD: 0.002 mm; LR: 0.8855 kN	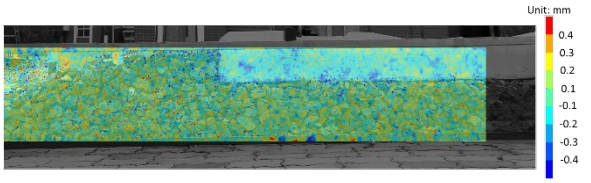 SD: 0.012 mm; LR: 0.88505
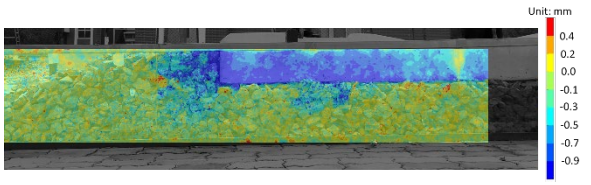 SD: 0.033 mm; LR: 2.0987	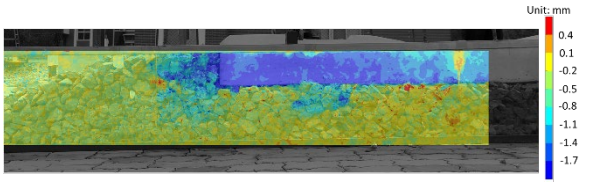 SD: 0.046 mm; LR: 2.364
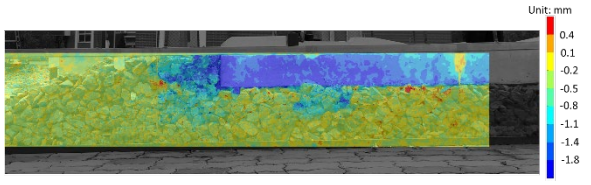 SD: 0.072 mm; LR: 2.625	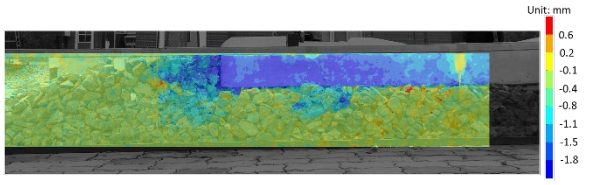 SD: 0.802 mm; LR: 2.962
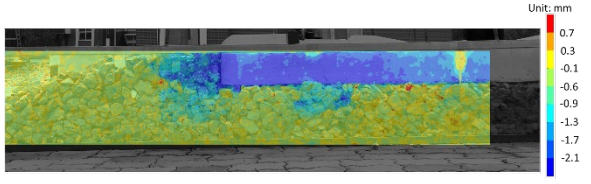 SD: 1.3886 mm; LR: 2.988	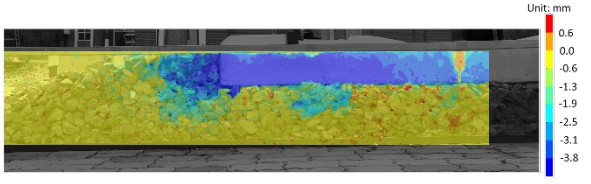 SD: 1.582 mm; LR: 3.062
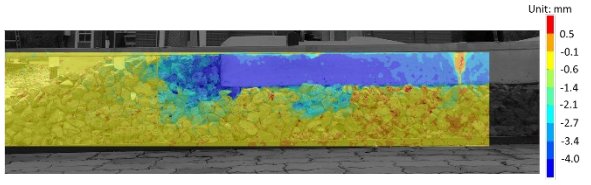 SD: 1.687 mm; LR: 3.077	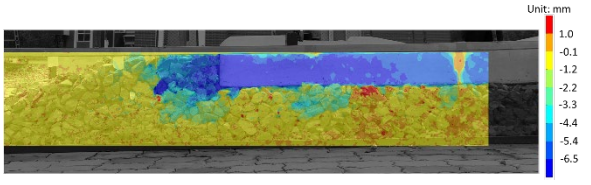 SD: 2.564 mm; LR: 3.374
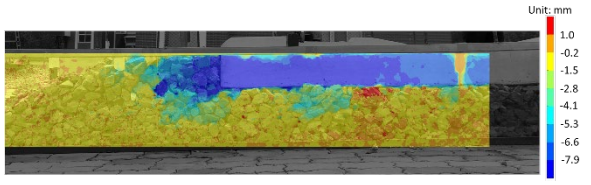 SD: 4.339 mm; LR: 3.605	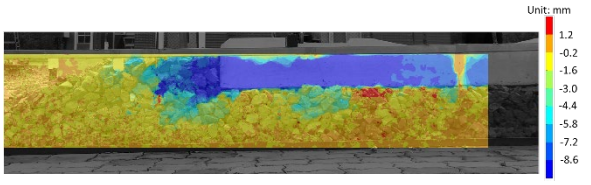 SD: 7.142 mm; LR: 3.522
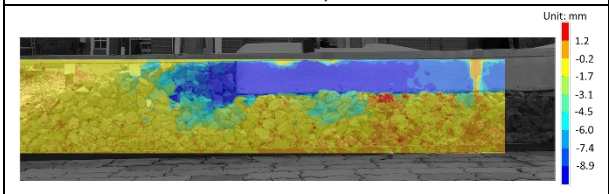 SD: 7.143 mm; LR: 3.654	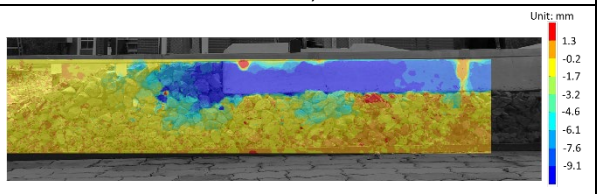 SD: 7.233 mm; LR: 3.654
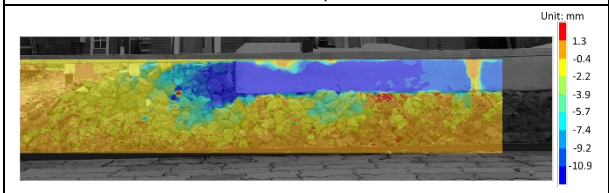 SD: 10.067 mm; LR: 3.794	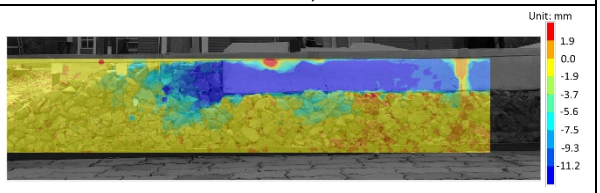 SD: 10.089 mm; LR: 3.766

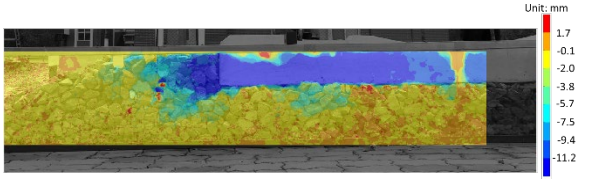 SD: 12.945 mm; LR: 3.838	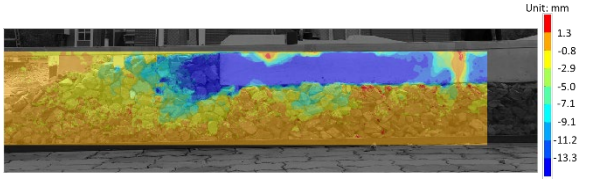 SD: 15.878 mm; LR: 3.994
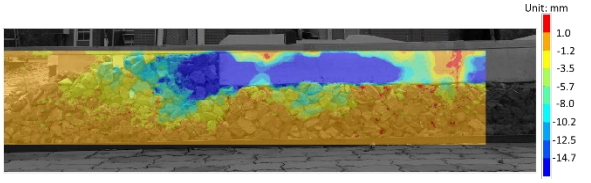 SD: 18.574 mm; LR: 3.883	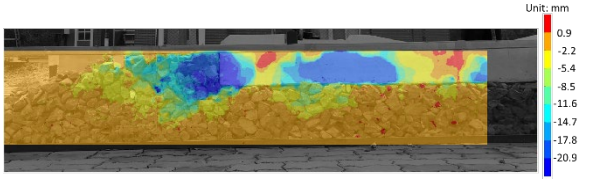 SD: 21.789 mm; LR: 4.005

Table A. 2 Vertical displacements of ballast particles at ballast bed cross section (SD-sleeper displacement; LR-lateral resistance)

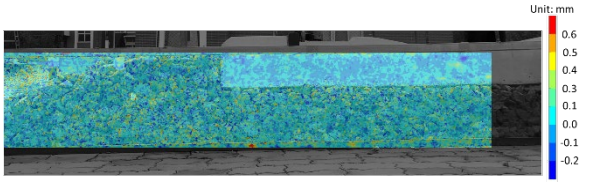 SD: 0.002 mm; LR: 0.8855 kN	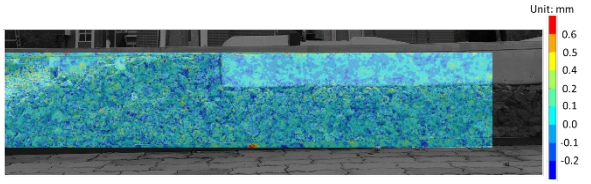 SD: 0.012 mm; LR: 0.88505
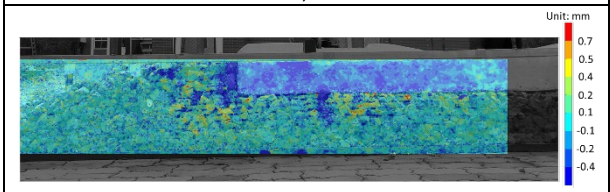 SD: 0.033 mm; LR: 2.0987	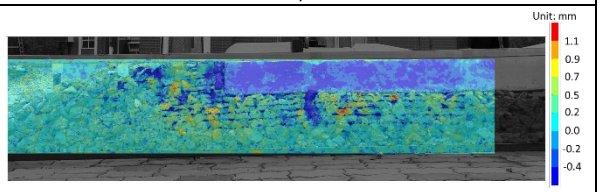 SD: 0.046 mm; LR: 2.364
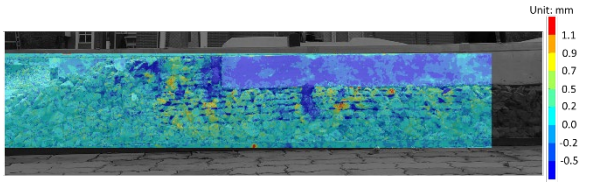 SD: 0.072 mm; LR: 2.625	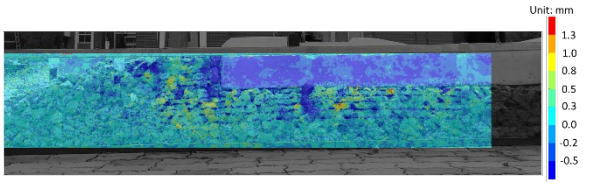 SD: 0.802 mm; LR: 2.962
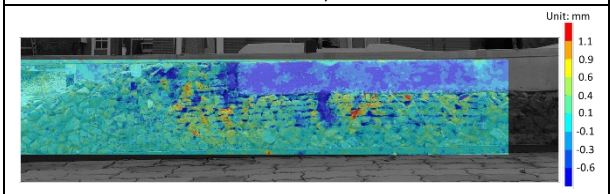 SD: 1.3886 mm; LR: 2.988	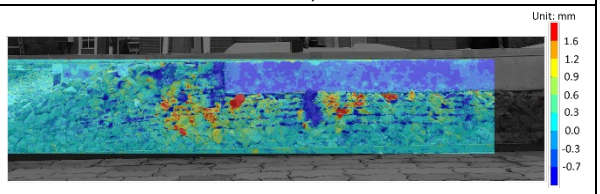 SD: 1.582 mm; LR: 3.062
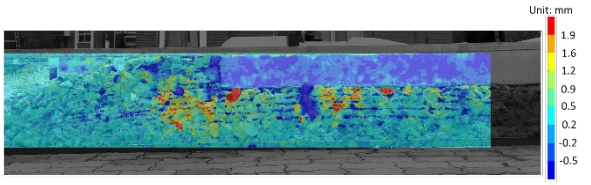 SD: 1.687 mm; LR: 3.077	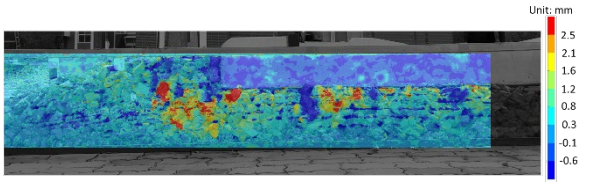 SD: 2.564 mm; LR: 3.374
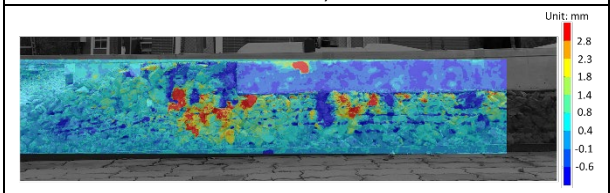 SD: 4.339 mm; LR: 3.605	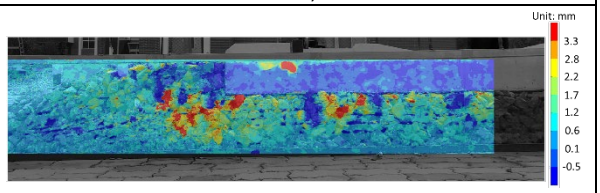 SD: 7.142 mm; LR: 3.522

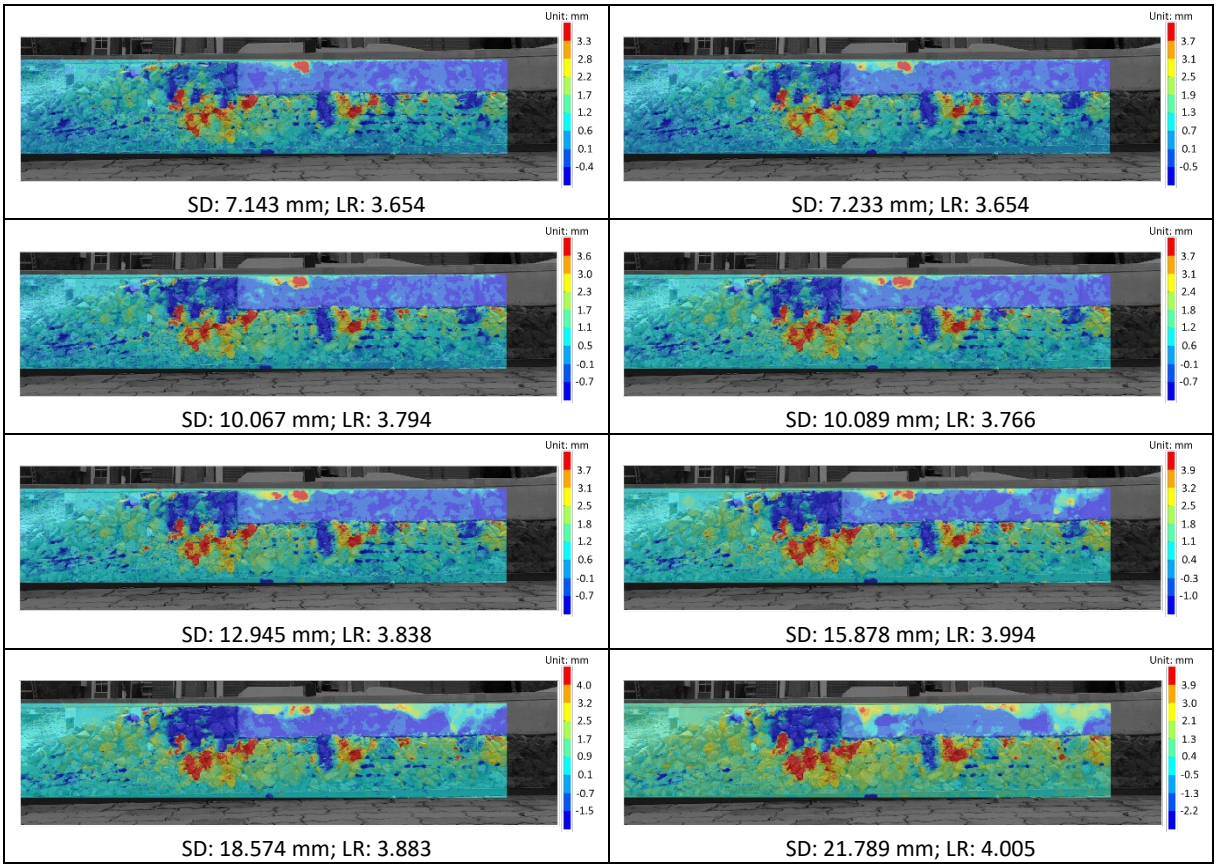

Table A. 3 Horizontal displacements of ballast particles at ballast shoulder (SD-sleeper displacement; LR-lateral resistance)

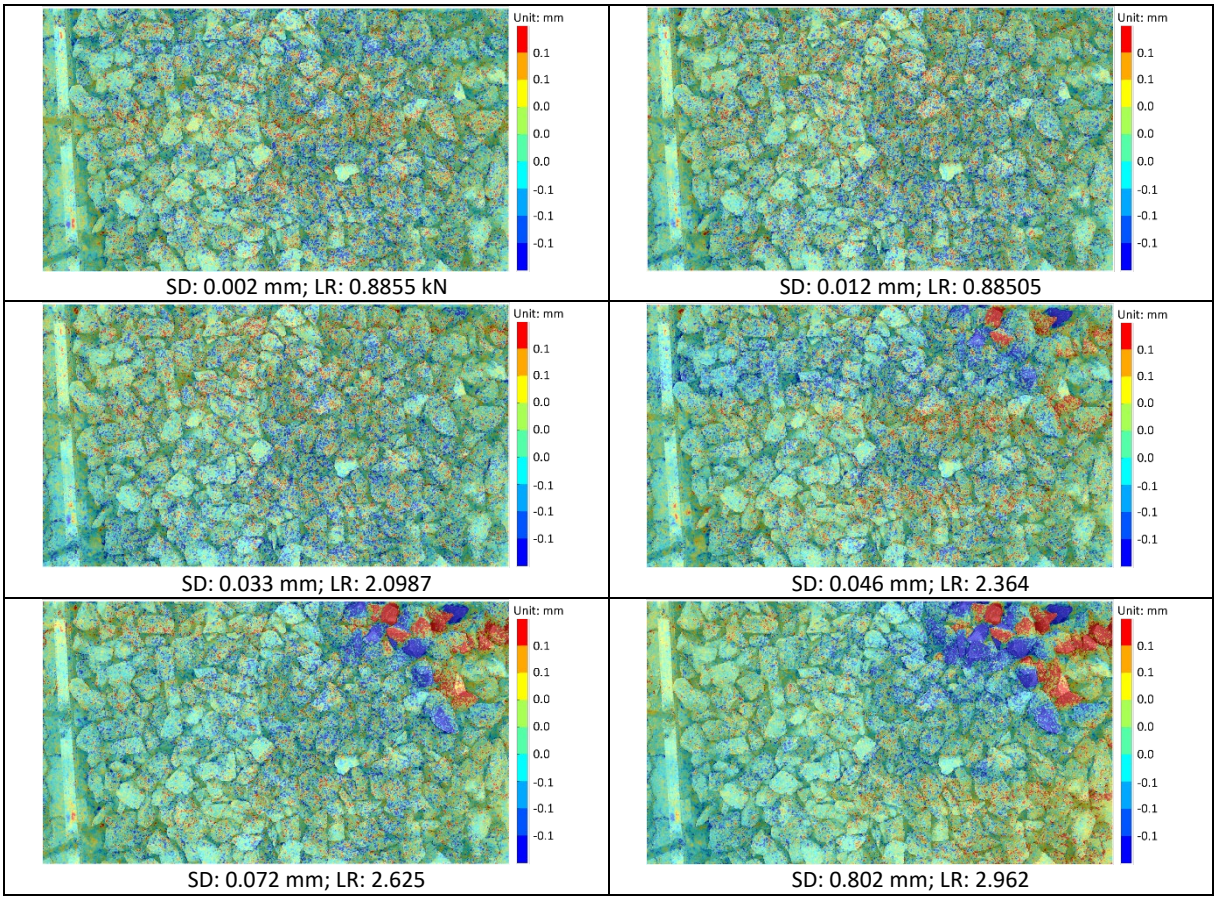

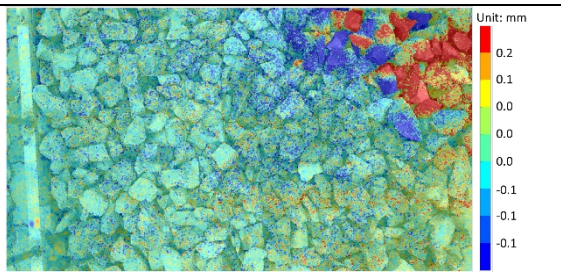

SD: 1.3886 mm; LR: 2.988

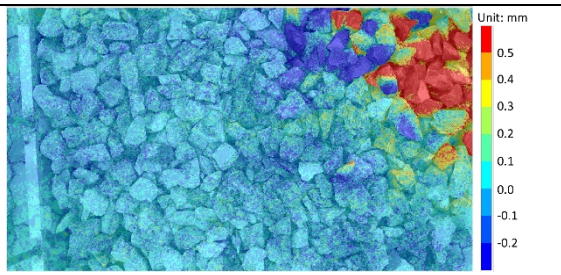

SD: 1.582 mm; LR: 3.062

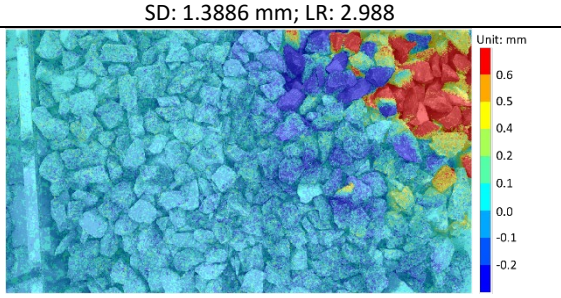

SD: 1.687 mm; LR: 3.077

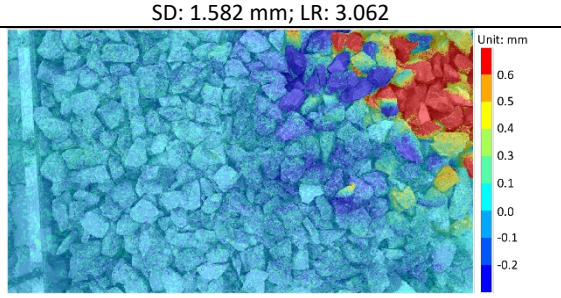

SD: 2.564 mm; LR: 3.374

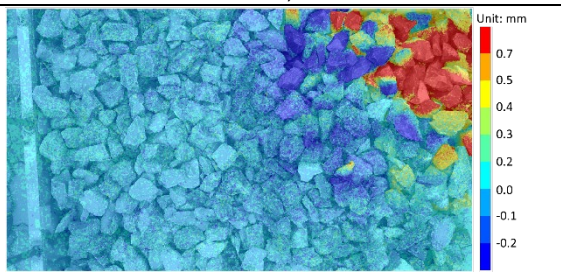

SD: 4.339 mm; LR: 3.605

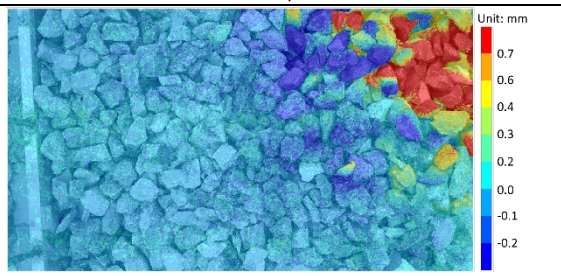

SD: 7.142 mm; LR: 3.522

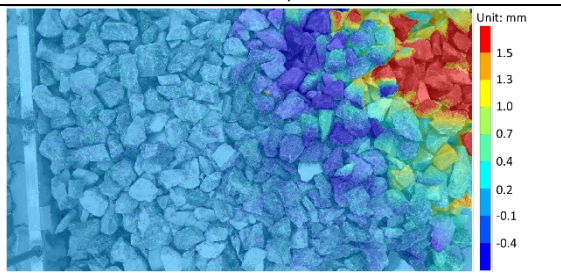

SD: 7.143 mm; LR: 3.654

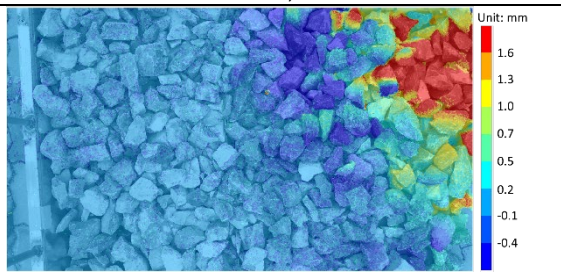

SD: 7.233 mm; LR: 3.654

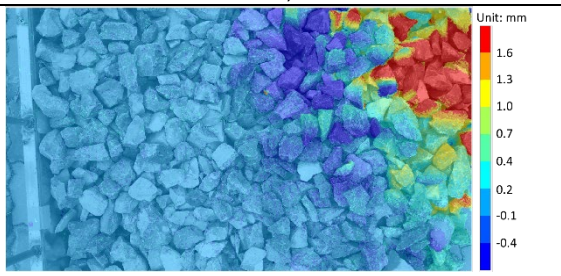

SD: 10.067 mm; LR: 3.794

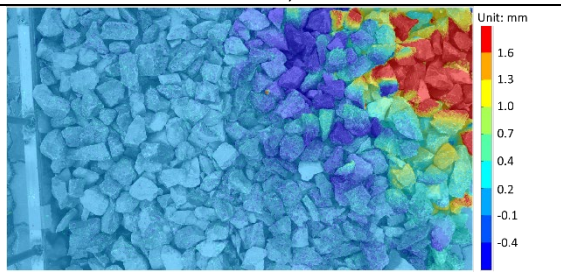

SD: 10.089 mm; LR: 3.766

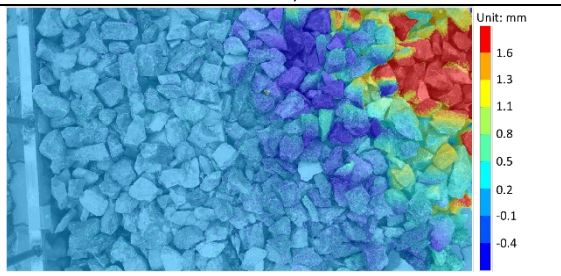

SD: 12.945 mm; LR: 3.838

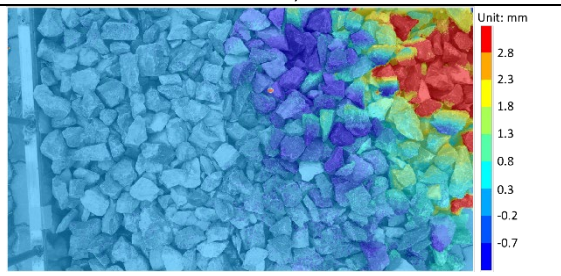

SD: 15.878 mm; LR: 3.994

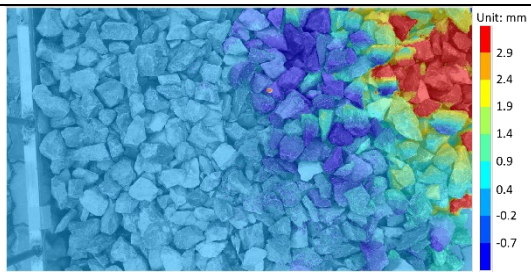 SD: 18.574 mm; LR: 3.883	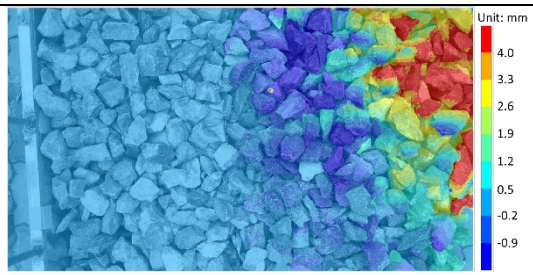 SD: 21.789 mm; LR: 4.005

Table A. 4 Vertical displacements of ballast particles at ballast shoulder (SD-sleeper displacement; LR-lateral resistance)

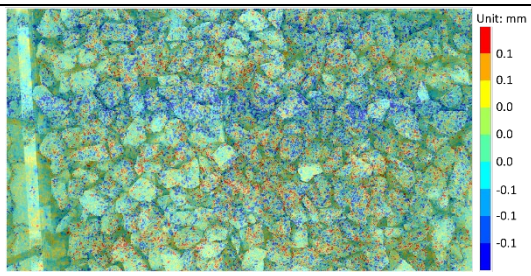 SD: 0.002 mm; LR: 0.8855 kN	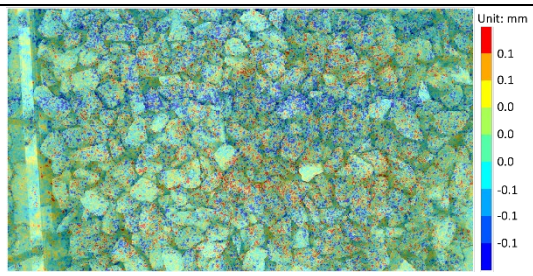 SD: 0.012 mm; LR: 0.88505
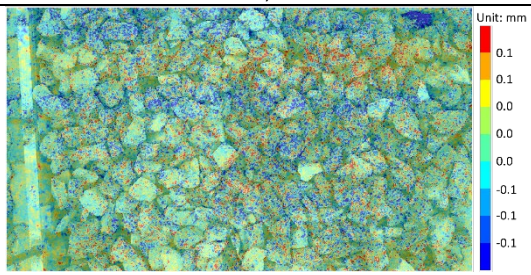 SD: 0.033 mm; LR: 2.0987	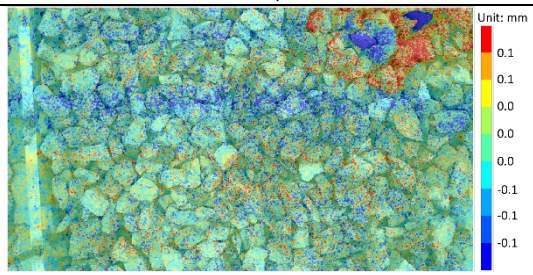 SD: 0.046 mm; LR: 2.364
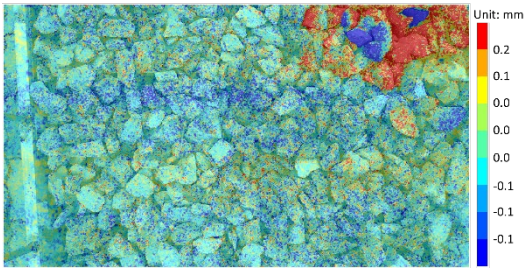 SD: 0.072 mm; LR: 2.625	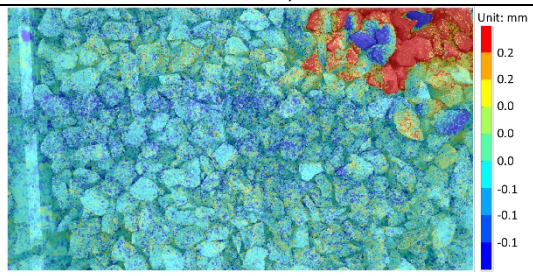 SD: 0.802 mm; LR: 2.962
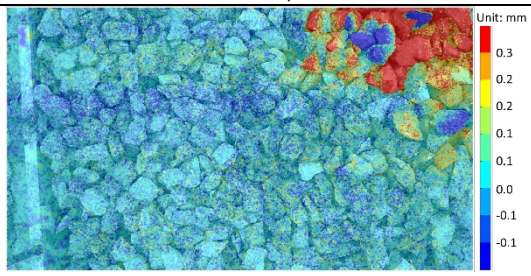 SD: 1.3886 mm; LR: 2.988	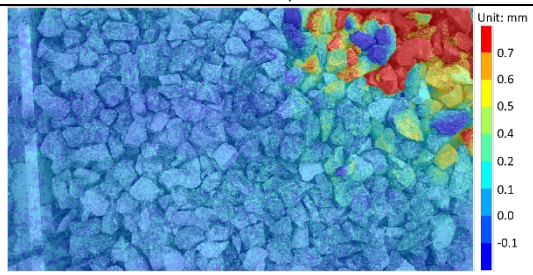 SD: 1.582 mm; LR: 3.062
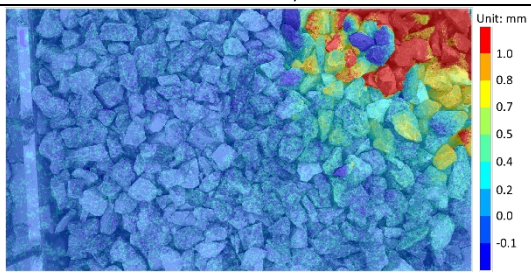 SD: 1.687 mm; LR: 3.077	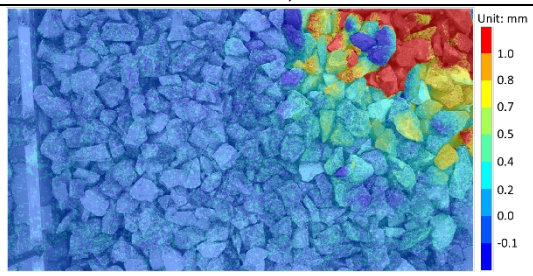 SD: 2.564 mm; LR: 3.374

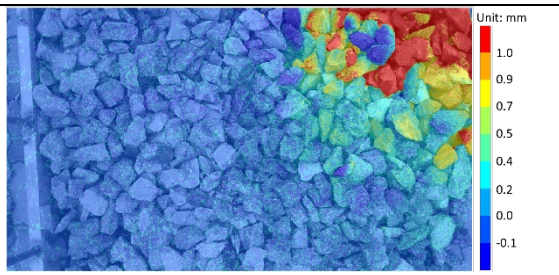 SD: 4.339 mm; LR: 3.605	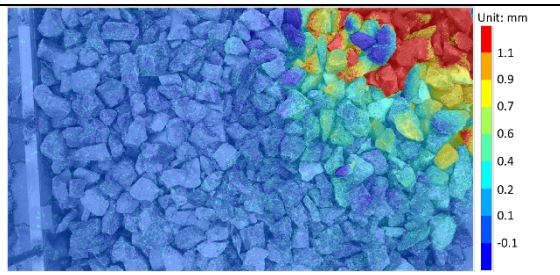 SD: 7.142 mm; LR: 3.522
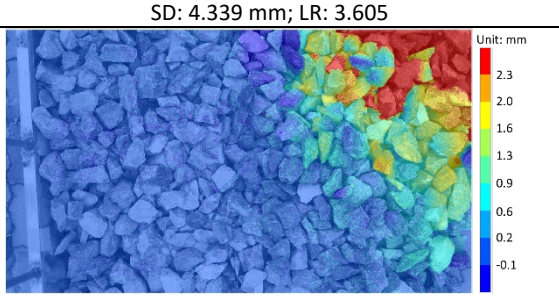 SD: 7.143 mm; LR: 3.654	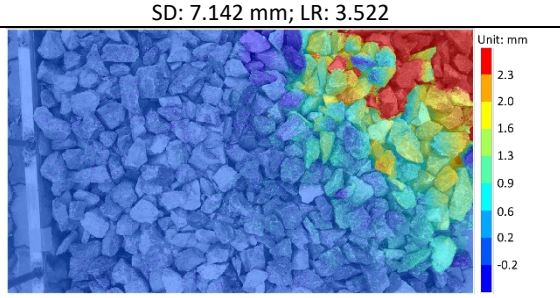 SD: 7.233 mm; LR: 3.654
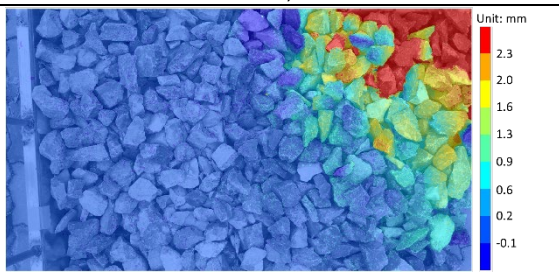 SD: 10.067 mm; LR: 3.794	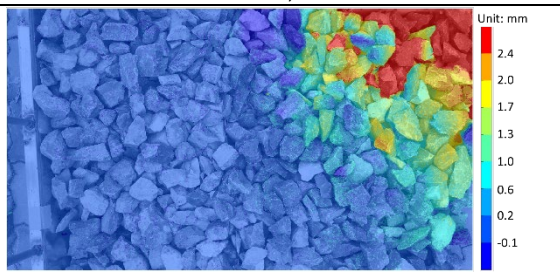 SD: 10.089 mm; LR: 3.766
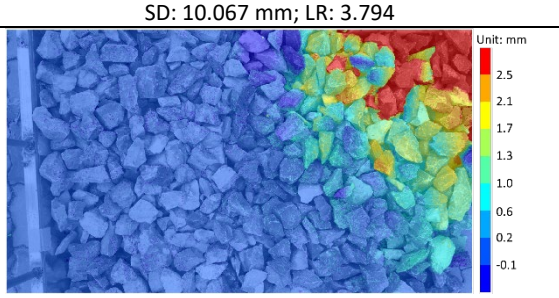 SD: 12.945 mm; LR: 3.838	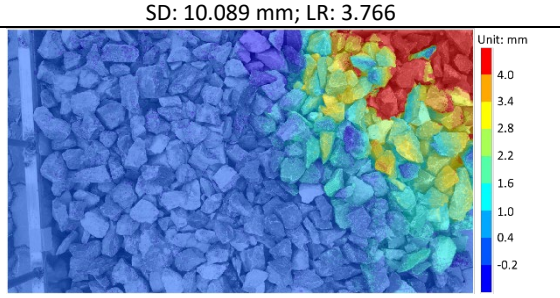 SD: 15.878 mm; LR: 3.994
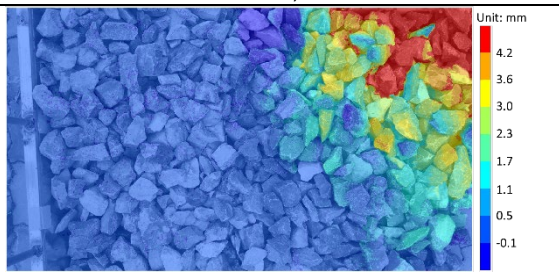 SD: 18.574 mm; LR: 3.883	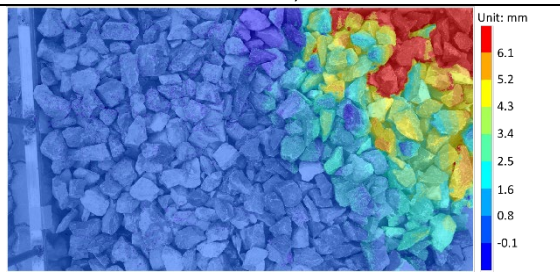 SD: 21.789 mm; LR: 4.005

Table A. 5 Comparison of ballast particle displacements between DEM results and PIV results at the sleeper displacement at 0.002 mm

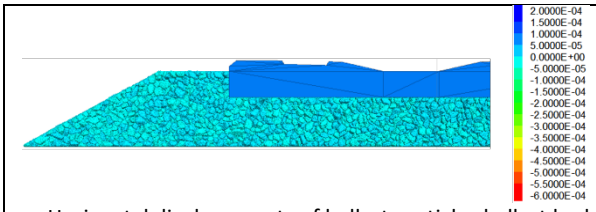 a. Horizontal displacements of ballast particles ballast bed cross section (DEM)	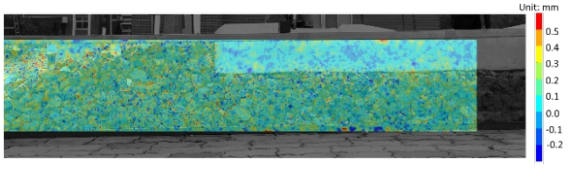 b. Horizontal displacements of ballast particles at ballast bed cross section (PIV)

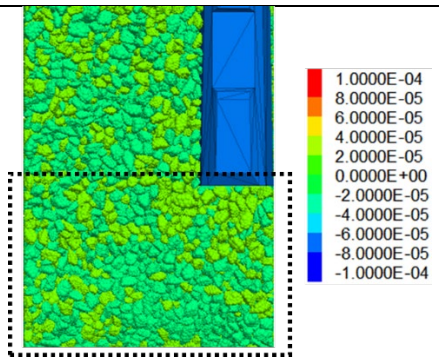

c. Horizontal displacements of ballast particles at ballast shoulder (DEM)

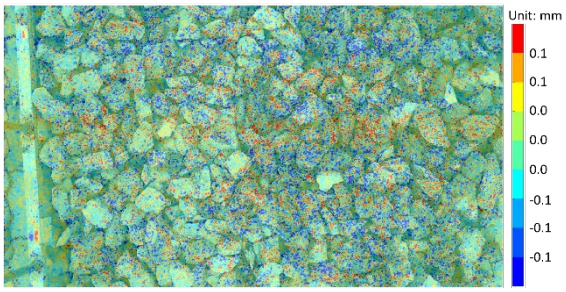

d. Horizontal displacements of ballast particles at ballast shoulder (PIV)

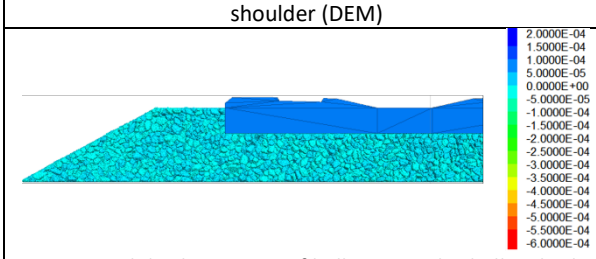

e. Vertical displacements of ballast particles ballast bed cross section (DEM)

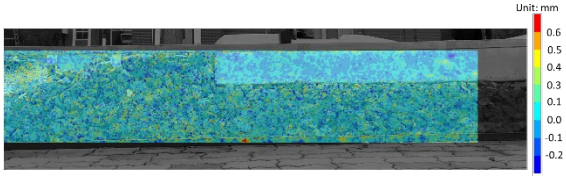

f. Vertical displacements of ballast particles at ballast bed cross section (PIV)

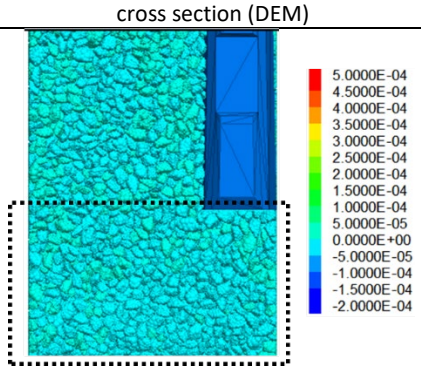

g. Vertical displacements of ballast particles at ballast shoulder (DEM)

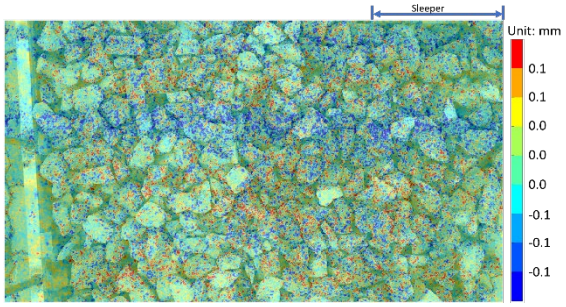

h. Vertical displacements of ballast particles at ballast shoulder (PIV)

Table A. 6 Comparison of ballast particle displacements between DEM results and PIV results at the sleeper displacement at 10.089 mm

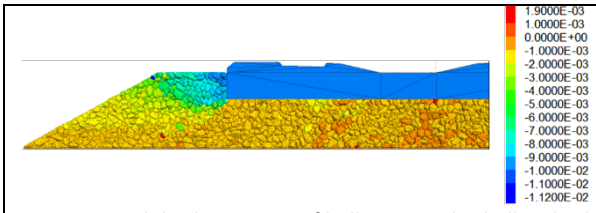

a. Horizontal displacements of ballast particles ballast bed cross section (DEM)

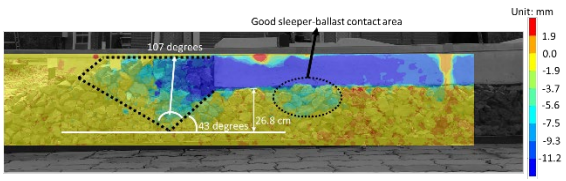

b. Horizontal displacements of ballast particles at ballast bed cross section (PIV)

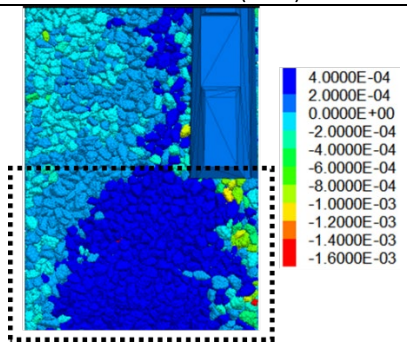

c. Horizontal displacements of ballast particles at ballast shoulder (DEM)

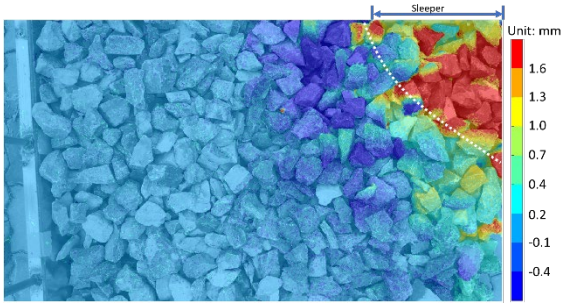

d. Horizontal displacements of ballast particles at ballast shoulder (PIV)

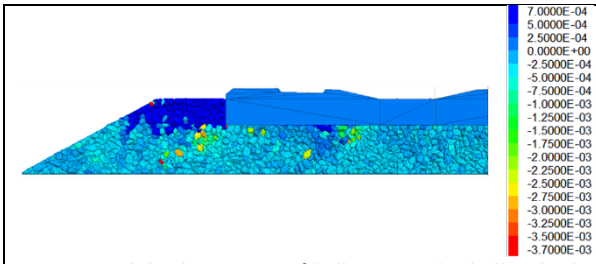

e. Vertical displacements of ballast particles ballast bed cross section (DEM)

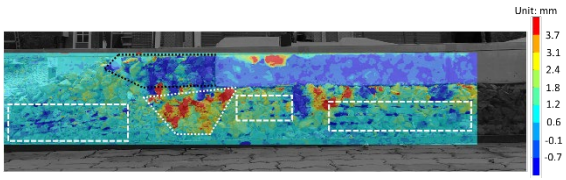

f. Vertical displacements of ballast particles at ballast bed cross section (PIV)

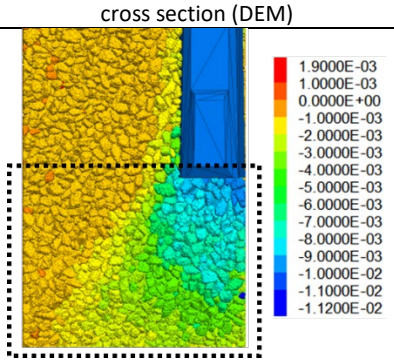

g. Vertical displacements of ballast particles at ballast shoulder (DEM)

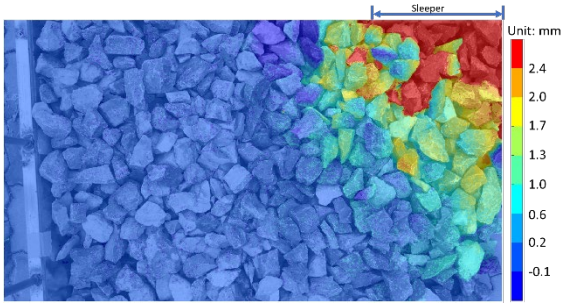

h. Vertical displacements of ballast particles at ballast shoulder (PIV)

Table A. 7 Comparison of ballast particle displacements between DEM results and PIV results at the sleeper displacement at 21.789 mm

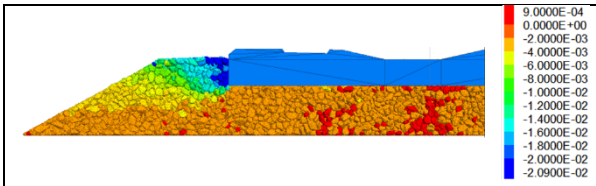

a. Horizontal displacements of ballast particles ballast bed cross section (DEM)

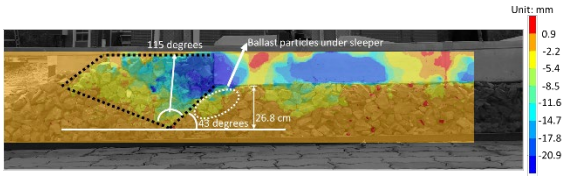

b. Horizontal displacements of ballast particles at ballast bed cross section (PIV)

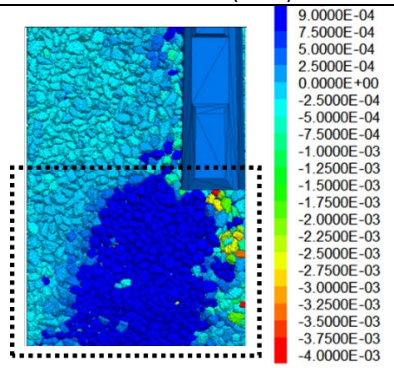

c. Horizontal displacements of ballast particles at ballast shoulder (DEM)

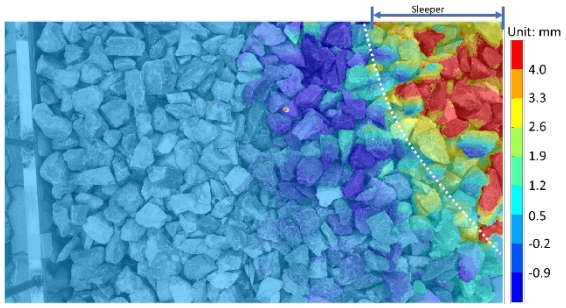

d. Horizontal displacements of ballast particles at ballast shoulder (PIV)

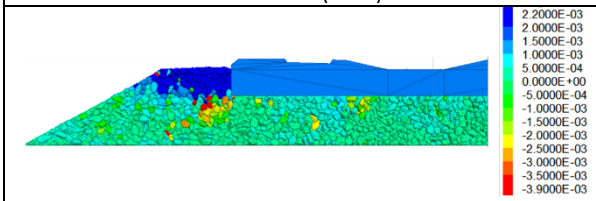

e. Vertical displacements of ballast particles ballast bed cross section (DEM)

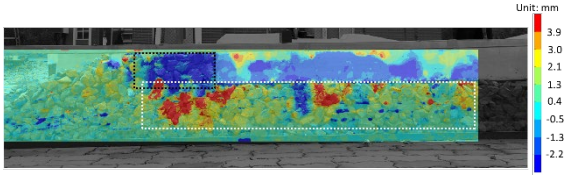

f. Vertical displacements of ballast particles at ballast bed cross section (PIV)

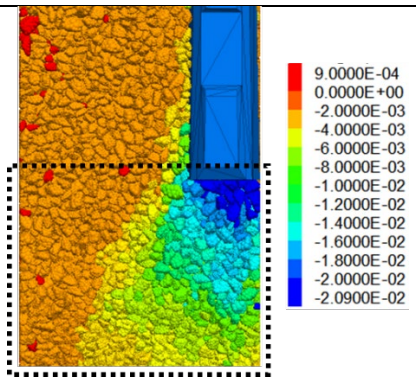

g. Vertical displacements of ballast particles at ballast shoulder (DEM)

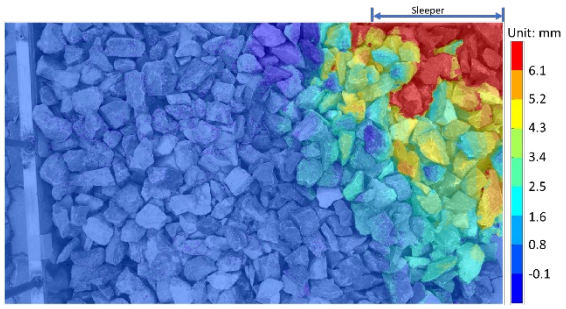

h. Vertical displacements of ballast particles at ballast shoulder (PIV)